Simulation of the Downshear Reformation of a Tropical Cyclone

LEON T. NGUYEN AND JOHN MOLINARI

Department of Atmospheric and Environmental Sciences, University at Albany, State University of New York, Albany, New York

(Manuscript received 2 February 2015, in final form 3 August 2015)

ABSTRACT

The downshear reformation of Tropical Storm Gabrielle (2001) was simulated at 1-km horizontal resolution using the Weather Research and Forecasting (WRF) Model. The environmental shear tilted the initial parent vortex downshear left and forced azimuthal wavenumber-1 kinematic, thermodynamic, and convective asymmetries. The combination of surface enthalpy fluxes and a lack of penetrative downdrafts right of shear allowed boundary layer moist entropy to increase to a maximum downshear right. This contributed to convective instability that fueled the downshear convection. Within this convection, an intense mesovortex rapidly developed, with maximum boundary layer relative vorticity reaching $2.2 \times 10^{-2}\,s^{-1}$. Extreme vortex stretching played a key role in the boundary layer spinup of the mesovortex. Cyclonic vorticity remained maximized in the boundary layer and intensified upward with the growth of the convective plume.

The circulation associated with the mesovortex and adjacent localized cyclonic vorticity anomalies comprised a developing ''inner vortex'' on the downshear-left (downtilt) periphery of the parent cyclonic circulation. The inner vortex was nearly upright within a parent vortex that was tilted significantly with height. This inner vortex became the dominant vortex of the system, advecting and absorbing the broad, tilted parent vortex. The reduction of tropical cyclone (TC) vortex tilt from 65 to 20 km in 3 h reflected the emerging dominance of this upright inner vortex. The authors hypothesize that downshear reformation, resulting from diabatic heating associated with asymmetric convection, can aid the TC's resistance to shear by reducing vortex tilt and by enabling more diabatic heating to occur near the center, a region known to favor TC intensification.

1. Introduction

Over the past few decades, tropical cyclone (TC) intensity forecasts have experienced slower improvement compared to tropical cyclone track forecasts (DeMaria et al. 2014). Several environmental factors have been shown to be associated with tropical cyclone intensification, including weak environmental vertical wind shear, high oceanic heat content, high low-to-midtropospheric relative humidity, and convective symmetry (Kaplan et al. 2010). Recently, through an ensemble of convection-permitting simulations, Zhang and Tao (2013) found that the predictability of tropical cyclone intensity declined with increasing environmental vertical wind shear. Their study highlights the necessity of understanding how tropical cyclones interact with environmental vertical wind shear.

Environmental vertical wind shear has been hypothesized to detrimentally affect tropical cyclone intensity through several proposed mechanisms. Frank and Ritchie (2001) argued that shear weakens the TC by ventilating the upper-level warm core, resulting in rising surface pressure following hydrostatic arguments. Simpson and Riehl (1958) and Tang and Emanuel (2010) suggested that ventilation of the TC core would be particularly effective in the middle troposphere owing to the sharper radial gradient in moist entropy. This ventilation could occur via vortex Rossby waves excited by the TC's interaction with vertical wind shear. Recently, Riemer et al. (2010) proposed that shear could affect TC intensity via thermodynamic modification of the inflow layer. In their simulation, the shear tilted the vortex, resulting in a quasi-stationary azimuthal wavenumber-1 convective asymmetry outside the eyewall region. Persistent downdrafts left of shear, resulting from evaporation of precipitation in unsaturated air, transported low-entropy air downward into the boundary layer. This entropy-depleted air was then carried inward and was unable to recover sufficiently via surface

Corresponding author address: Leon T. Nguyen, Department of Atmospheric and Environmental Sciences, ES 325, University at Albany, SUNY, 1400 Washington Ave, Albany, NY 12222.
E-mail: lnguyen@albany.edu

DOI: 10.1175/JAS-D-15-0036.1

enthalpy fluxes before reaching the eyewall region, resulting in a reduction of eyewall entropy and subsequent weakening of the TC. These aforementioned mechanisms are not necessarily mutually exclusive, and the relative importance of each of these mechanisms has yet to be assessed and quantified in observations.

Vertical wind shear acts to tilt the tropical cyclone vortex preferentially toward the downshear-left direction, as predicted by theory (e.g., Jones 1995; Reasor et al. 2004) and supported by model simulations (e.g., Braun et al. 2006; Riemer et al. 2010) and observations (e.g., Reasor et al. 2013). This TC vortex tilt is often accompanied by an azimuthal wavenumber-1 vertical motion and convective asymmetry, which has been well-documented in modeling (e.g., Braun et al. 2006; Riemer et al. 2010) and observational (e.g., Corbosiero and Molinari 2002; Chen et al. 2006; Reasor et al. 2013) studies of sheared TCs. The resiliency of TC vortices to shear has been hypothesized to occur through precession as a result of the vertically penetrating flow of the tilted vortex (Jones 1995) or through vortex Rossby wave damping (Reasor and Montgomery 2001; Reasor et al. 2004). Diabatic heating can aid the resiliency of the vortex in several ways. The reduced static stability can enhance the vertical coupling between the upper and lower vortices, resulting in an increased precession frequency and reduction of the tilt (Jones 1995). Also, the axisymmetric component of the secondary circulation induced by the diabatic heating can increase the radial PV gradient and Rossby number, increasing the efficiency of the vortex Rossby wave damping mechanism (Reasor et al. 2004).

Diabatic processes may also help the vortex resist shear through the process of downshear reformation. TC Danny (1997) was one such example (Molinari et al. 2004). TC Danny experienced 5–11 m s^{-1} of 850–200-hPa environmental vertical wind shear, resulting in a highly asymmetric convective structure. Over a period of several hours, the TC center, which was initially displaced upshear of the convection, reformed underneath the downshear convection according to satellite and surface observations. Satellite observations during the ensuing hours suggested that this new center became the dominant vortex in the system. TC Gabrielle (2001) was another observed case of downshear reformation (Molinari et al. 2006; Molinari and Vollaro 2010). The center of Gabrielle reformed adjacent to an intense downshear convective cell. During this reformation, the minimum surface pressure estimated from aircraft reconnaissance fell 22 hPa in less than 3 h. The new vortex was nearly upright and embedded within a broader vortex that was tilted left of the shear vector. Molinari and Vollaro (2010) noted that this intense convective cell bore some resemblance to vortical hot towers (VHTs), convective plumes possessing intense cyclonic vorticity (Hendricks et al. 2004). Such structures have been observed in predepression tropical disturbances as well as tropical cyclones (e.g., Houze et al. 2009; Bell and Montgomery 2010). VHTs are hypothesized to play an important role in tropical cyclogenesis and tropical cyclone intensification through their merger and axisymmetrization and collectively through their diabatically induced secondary circulation that converges absolute angular momentum (e.g., Montgomery et al. 2006; Montgomery and Smith 2012). Although many numerical modeling studies have explored the characteristics and evolution of VHTs as well as their contribution to TC genesis and intensification (e.g., Hendricks et al. 2004; Montgomery et al. 2006; Van Sang et al. 2008), these studies typically involve an upright vortex with no imposed relative flow. Recently, Kilroy and Smith (2013) and Kilroy et al. (2014) explored the characteristics and behavior of VHTs in a vertically and horizontally sheared local environment using an idealized modeling framework. The characteristics and behavior of VHTs in sheared, tilted TCs, and their role, if any, in helping the TC counteract shear remain topics to be further explored.

When downshear reformation occurs, the new vortex can be small and can form in the span of just a few hours. This makes downshear reformation very difficult to observe in nature owing to the spatial and temporal limitations of observations. Thus, it is not currently known how often downshear reformation cases like Danny (1997) and Gabrielle (2001) actually occur. However, the advent of cloud-resolving models and increased computational resources make it possible to simulate such events. To the extent that these simulations can approximate nature, they can be used to better understand specifically the physical processes behind downshear reformation and, more broadly, the interaction of tropical cyclones with environmental vertical wind shear.

The current study analyzes a simulation of the downshear reformation event of Gabrielle (2001). This paper will be organized as follows. In section 2, the model setup will be described. A broad overview of the environmental conditions will be given in section 3. Section 4 will explore the development of TC-scale asymmetries in response to the environmental shear. The evolution of a small-scale vortex that formed downshear of the initial TC center will be discussed in sections 5 and 6. Section 7 will explore the interaction between this intense small-scale vortex, adjacent localized cyclonic vorticity anomalies, and the broad parent vortex, as well as the subsequent reduction in TC vortex

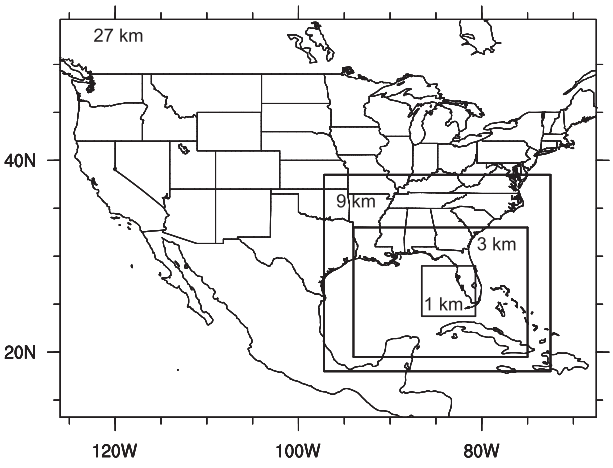

FIG. 1. Map of the model domain setup.

tilt. A summary of these results and further speculations will be presented in section 8.

2. Methods

As in Nguyen et al. (2014), the Weather Research and Forecasting (WRF) Model, version 3.2 (Skamarock et al. 2008), was used to simulate the downshear reformation of Gabrielle. Four nested domains of 27-, 9-, 3-, and 1-km horizontal resolution were used (Fig. 1). The 27- and 9-km domains were initialized at 1200 UTC 13 September, the 3-km domain was initialized at 1800 UTC 13 September, and the 1-km domain was initialized at 0000 UTC 14 September. The National Centers for Environmental Prediction (NCEP) Global Forecast System (GFS) final (FNL) operational global analyses were used for initial conditions and boundary conditions.

The model physics parameterizations used were as follows: the Kain–Fritsch cumulus parameterization on the 27- and 9-km domains (Kain and Fritsch 1993), the WRF single-moment 6-class microphysics scheme (Hong and Lim 2006), the Dudhia shortwave radiation (Dudhia 1989) and the Rapid Radiative Transfer Model longwave radiation (Mlawer et al. 1997) schemes, and the Yonsei University planetary boundary layer scheme (Noh et al. 2003).

Following Nguyen et al. (2014), the tropical cyclone center was defined by the centroid of the sea level pressure field over a circular region representative of the TC inner core. Weaker TCs often contain small-scale convective cells and associated cyclonic vorticity anomalies. These localized features are not representative of the TC vortex but can nonetheless influence the analyzed TC center position. The pressure centroid method was used because it was less sensitive to these features. The vortex tilt was determined using the pressure centroids at multiple vertical levels.

3. Overview of simulation and environmental conditions

Figure 2 shows the track of the storm in the WRF simulation (solid line) compared to observations from aircraft reconnaissance (dashed line) between 0000 and 1200 UTC 14 September. Although the simulated track was displaced about 50 km northwest of the observed track, the north-northeastward motion was well captured. Figure 3 shows the simulated tropical cyclone intensity evolution during the 6-h period of interest (0000–0600 UTC 14 September). The simulated maximum 10-m wind speed increased from 25–28 to 36–39 m s^{-1}, while the minimum sea level pressure dropped from 995 to 984 hPa. Sea surface temperatures, ranging between 29.5° and 30.0°C, were sufficiently warm for intensification. The 850–200-hPa vertical wind shear, averaged within 500 km of the TC center, was from the west-southwest at 9–10 m s^{-1} during the 6-h period. This compared well with the shear computed using ECMWF gridded analysis by Molinari et al. (2006). However, simply computing the vector difference between two vertical levels may not capture the variability of the environmental wind with height (DeMaria 2010). To address this, Fig. 4 shows a hodograph of the wind averaged within 500 km of the TC center up to 12-km height. The environmental wind shear was present throughout the depth of the troposphere and was not confined to a particular layer. The hodograph exhibited a clockwise curvature below 4 km and a counterclockwise curvature above 4 km, indicative of positive and negative TC-relative environmental helicity, respectively. Nolan (2011) and Onderlinde and Nolan (2014) hypothesized that tropical cyclones embedded within a deep layer of positive TC-relative environmental helicity were more likely to intensify, although they did not investigate situations in which the helicity changed sign with height, as in this case.

4. Shear-induced asymmetries

The vertical shear of the environmental flow acted to tilt the tropical cyclone vortex. Figure 5 shows the pressure and wind fields at the surface and the 8-km height levels, along with TC center positions at different altitudes. The TC was tilted persistently in the downshear-left direction with height, consistent with theory, modeling, and observations, as noted in the introduction. An anticyclonic turning with height of the vortex tilt was also evident. This tilt structure was subtly

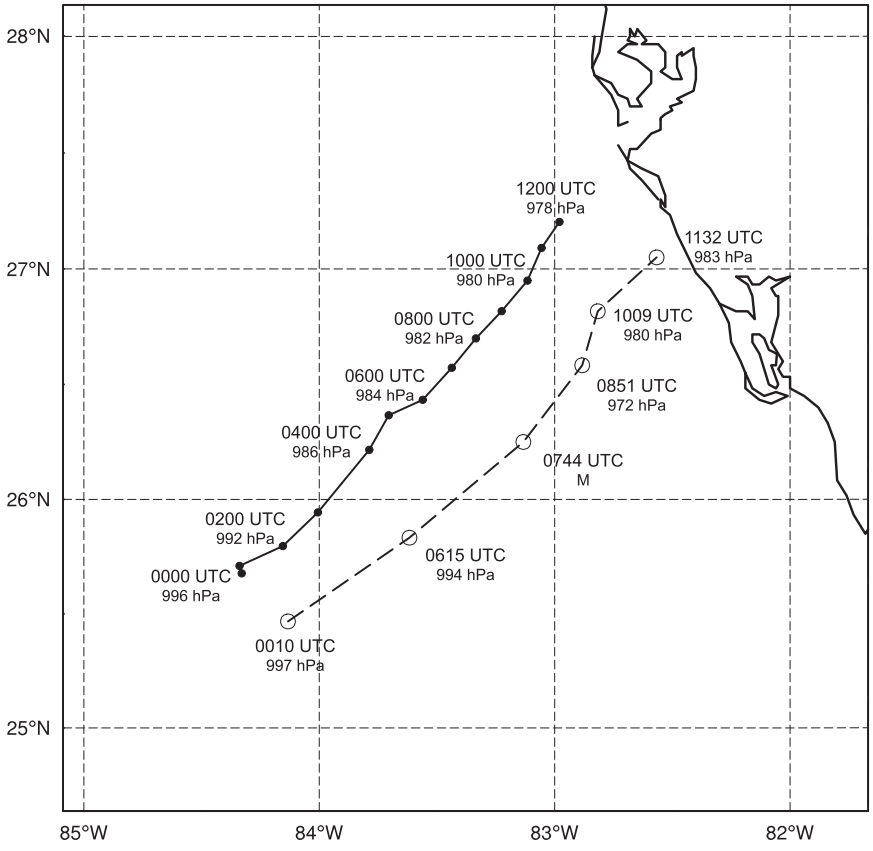

FIG. 2. Simulated (1-h resolution; solid line) and observed (dashed line) TC track between 0000 and 1200 UTC 14 Sep. Accompanying the tracks are minimum sea level pressures at the given times.

hinted at in a tilt composite using airborne dual-Doppler data in sheared, mature TCs (Reasor et al. 2013). Whether this curvature reflects the TC vortex response to the environmental hodograph (Fig. 4) or a response inherent to baroclinic vortices as suggested by Jones (2000) remains unresolved. Figure 6 shows the shear-relative quadrant-averaged potential temperature perturbation from the azimuthal mean at 500-km radius (color fill) and asymmetric potential temperature perturbation (contours). The warm core was maximized at about 8-km height, reached a magnitude of nearly 7 K, and was displaced toward the downshear-left direction. Below 5-km height, the potential temperature was 1–3 K cooler downshear left (downtilt) than upshear right (uptilt). In dry idealized simulations, Jones (1995) showed that a balanced thermal asymmetry developed in response to the vortex tilt, with cooling (warming) occurring downtilt (uptilt). Diabatic heating associated with convection can counteract this adiabatic cooling downtilt (Frank and Ritchie 1999), although to what extent remains to be seen. A downtilt cold anomaly was found in a full-physics simulation of Hurricane Bonnie (1998) (Braun et al. 2006) and in observations of Hurricane Guillermo (1997) (Reasor and Eastin 2012). This may be the result of adiabatic cooling in updrafts slightly exceeding diabatic heating, as suggested by Zhang et al. (2002). Evaporative cooling associated with downdrafts also may have contributed to the downshear-left cool anomaly in the lower troposphere.

Figure 7 shows the evolution of sea level pressure and simulated reflectivity at 1-km height between 0230 and 0600 UTC 14 September. The reflectivity field exhibited a marked wavenumber-1 asymmetry, with much of the precipitation confined downshear and downshear left (downtilt). This asymmetry was consistent with observational (e.g., Corbosiero and Molinari 2002; Chen et al. 2006; Reasor et al. 2013) and numerical modeling studies (e.g., Braun et al. 2006; Riemer et al. 2010) of sheared tropical cyclones. A wavenumber-1 asymmetry in moist entropy and radial wind was also observed in the simulation. Figure 8 shows the shear-relative quadrant-averaged equivalent potential temperature θ_e, vertical motion, and radial wind during a representative 30-min time period. Upward motion

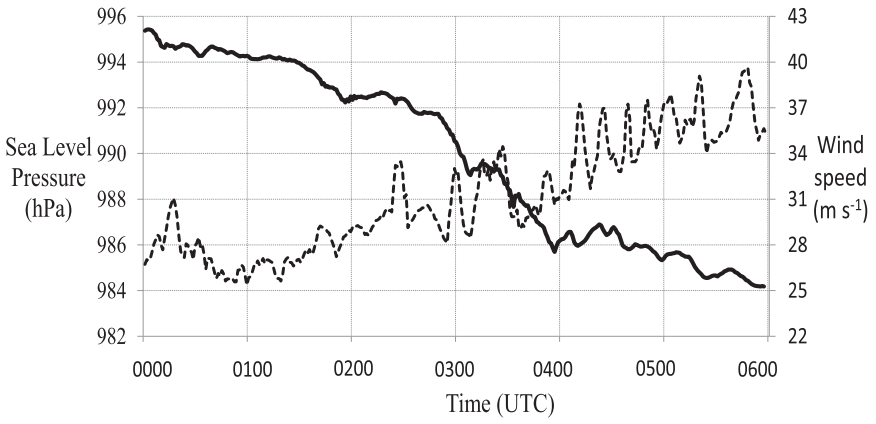

FIG. 3. Time series of the minimum sea level pressure (solid line; left axis) and maximum 10-m wind speed (dashed line; right axis).

associated with convection was confined primarily to the downshear quadrants, with weak downward motion prevalent in the upshear-left quadrant. In the lowest 2 km, inflow of up to 15 m s^{-1} was observed beneath and radially outward of the downshear convection, while in contrast, weak low-level outflow of 3 m s^{-1} was observed upshear left. In the mid-to-upper troposphere (4–10-km height), inflow of 10–15 m s^{-1} was observed upshear left extending well into the TC inner core, with outflow of 6–12 m s^{-1} observed right of shear. These results generally depicted enhanced in–up–out flow in the downshear quadrants and suppressed or even a reversal of in–up–out flow in the upshear quadrants, consistent with observational studies of TCs interacting with vertical wind shear (e.g., Reasor et al. 2013; DeHart et al. 2014).

Boundary layer θ_e reached a maximum downshear right and a minimum left of shear, with differences on the order of 5–7 K out to the 125-km radius. Midlevel θ_e (4–8-km height) was 10–15 K higher in the downshear-left quadrant than in the upshear quadrants. These moist entropy differences were consistent with the life cycle of updrafts and downdrafts in a sheared tropical cyclone, as discussed by Riemer et al. (2010) and Zhang et al. (2013). Air parcels associated with convection initiating downshear right ascended and were advected cyclonically into the downshear-left quadrant. This convection acted to moisten the midtroposphere downshear left. As convection matured downshear left, downdrafts driven by evaporating precipitation and water loading deposited low-entropy air into the low levels upshear left. The boundary layer θ_e was then able to recover via surface enthalpy fluxes until reaching a maximum downshear right. There, convection initiated once again, possibly aided by enhanced boundary layer convergence resulting from the tilt of the vortex, as suggested by Riemer et al. (2010).

Within the strongly sheared, tilted, and asymmetric parent tropical cyclone, a small-scale vortex (mesovortex) rapidly spun up and played a significant role in the intensification of the parent TC vortex. As seen in Figs. 5 and 7, this mesovortex initially formed downshear right, rapidly intensified as it revolved into the downshear and downshear-left quadrants, and then axisymmetrized with the TC vortex by 0600 UTC. The minimum sea level pressure of the mesovortex fell 5.4 hPa between 0255 and 0355 UTC (Fig. 3). Although this rate did not match the extreme deepening rate observed in nature (22 hPa in 2.6 h), the intense mesovortex was qualitatively similar to the one documented by Molinari and Vollaro (2010). The simulated reflectivity evolution (Fig. 7) showed close similarities to the observed reflectivity evolution (Fig. 6 in Molinari and Vollaro 2010). Also, the 700-hPa temperature spike and corresponding relative humidity minimum observed by aircraft reconnaissance (Fig. 12 in Molinari and Vollaro 2010) were also present in the simulation, although their magnitudes were reduced (not shown). These structural similarities give us confidence in the fidelity of the simulation. The dynamics of the intensification of this mesovortex will be explored in detail in the following sections, and the role of the TC-scale asymmetries in the rapid intensification (RI) of this mesovortex will also be discussed.

5. Mesovortex evolution: Vorticity

Figure 9 shows the relative vorticity, TC-relative winds, and vertical motion at 1-km height, focused primarily on the downshear and downshear-left portions of the storm. The mesovortex was associated with a local maximum of cyclonic relative vorticity reaching 8 × 10^{-3} s^{-1} and was adjacent to a 1-km updraft of 3 m s^{-1} at

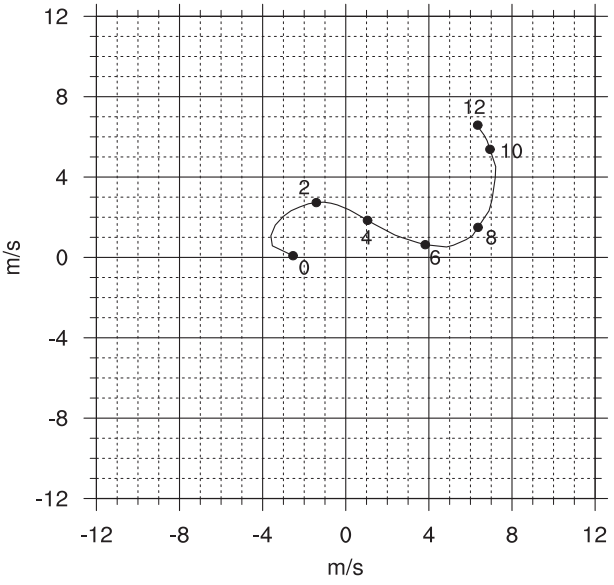

FIG. 4. Hodograph of the area-averaged wind within 500 km of the tropical cyclone center at 0300 UTC 14 Sep. Each dot represents a 2-km height increment, starting from the surface and ending at 12-km height.

0245 UTC 14 September (Fig. 9a). Over the next 30 min (Figs. 9b,c), cyclonic relative vorticity nearly tripled to $2.2 \times 10^{-2}\,s^{-1}$, nearly identical to the $2.5 \times 10^{-2}\,s^{-1}$ value in the observed storm (Molinari and Vollaro 2010). Meanwhile, the adjacent 1-km updraft also intensified to over $5\,m\,s^{-1}$. The cyclonic vorticity and the associated updraft continued to maintain their intensity through 0330 UTC 14 September (Fig. 9d). In addition to this intense mesovortex, there were many other cyclonic and anticyclonic vorticity anomalies on the downshear side of the TC. These couplets were generated through tilting of horizontal vorticity into the vertical by convective updrafts (e.g., Montgomery et al. 2006). Upon close inspection, the mesovortex was the most sustained and intense cyclonic vorticity anomaly during the simulation. This was likely due to its location inside the radius of maximum wind (RMW), which was 100–125 km during 0245–0330 UTC. Flow inside the RMW tends to be rotation dominated, whereas flow outside the RMW tends to be strain dominated (Rozoff et al. 2006). Thus, small-scale coherent structures such as mesovortices are more likely to last for long periods of time inside the RMW but are more likely to be filamented outside the RMW. Also, the local environment inside the RMW contained more cyclonic vorticity for the convective updraft to converge and stretch. Idealized experiments by Kilroy et al. (2014) showed that the maximum cyclonic vorticity associated with a convective updraft increased as the background rotation rate increased.

The intense cyclonic vorticity associated with the mesovortex was most concentrated in the low levels and appeared to build upward with time. Figure 10 shows west–east cross sections through the mesovortex center ($x = 0$) of relative vorticity, vertical motion, and mesovortex-relative flow during the period of rapid spinup. At 0235 UTC, prior to the rapid spinup (Fig. 10a), cyclonic vorticity over $2 \times 10^{-3}\,s^{-1}$ only reached up to the 3-km height. On the eastern flank of the mesovortex was a weak, shallow updraft that reached 2-km height. Directly over the mesovortex was a region of 1–2 $m\,s^{-1}$ subsidence that appeared to stunt the growth of the updraft. By 0250 UTC (Fig. 10b), the subsidence dissipated, and the shallow updraft began to intensify and accelerate upward. Fifteen minutes later (Fig. 10c), the updraft was 11 km in height and reached a maximum of over $10\,m\,s^{-1}$. The cyclonic relative vorticity in the lowest kilometer tripled, reaching over $2 \times 10^{-2}\,s^{-1}$. By 0320 UTC (Fig. 10d), the convective updraft reached the tropopause (15–16-km height), the cyclonic relative vorticity in the low levels remained intense, and the cyclonic relative vorticity in the midtroposphere (3–8-km height) increased to near $1 \times 10^{-3}\,s^{-1}$. The mesovortex was tilted slightly toward the east with height, as was the adjacent convective updraft. The updraft was most intense ($>20\,m\,s^{-1}$) in the upper troposphere, likely as a result of fusion heating contributing to parcel buoyancy (e.g., Romps and Kuang 2010; Molinari et al. 2012).

To explore the physical mechanisms responsible for the dramatic boundary layer spinup and the vertical growth of the mesovortex, we recall the tendency equation for the vertical component of absolute vorticity following Fang and Zhang (2010):

$$\left.\frac{\partial \zeta}{\partial t}\right|_{\mathrm{MV}} = -(\mathbf{V}_h - \mathbf{C}) \cdot \nabla_h(\zeta + f) - w\frac{\partial \zeta}{\partial z} - (\zeta + f)\nabla_h \cdot (\mathbf{V}_h - \mathbf{C}) - \left(\frac{\partial w}{\partial x}\frac{\partial v}{\partial z} - \frac{\partial w}{\partial y}\frac{\partial u}{\partial z}\right) + \frac{1}{\rho^2}\left(\frac{\partial \rho}{\partial x}\frac{\partial p}{\partial y} - \frac{\partial \rho}{\partial y}\frac{\partial p}{\partial x}\right) + \frac{\partial F_y}{\partial x} - \frac{\partial F_x}{\partial y}, \quad (1)$$

where ζ is the relative vorticity and $\mathbf{C}$ is the motion of the mesovortex, calculated over a 20-min window centered on the analysis time. The subscript MV denotes that this term is the vorticity tendency in a reference frame moving with the mesovortex. The terms on the right-hand side of the equation represent horizontal advection of absolute vorticity, vertical advection of absolute vorticity, stretching of absolute vorticity, and tilting of horizontal vorticity into the vertical, solenoidal, and subgrid-scale parameterizations,

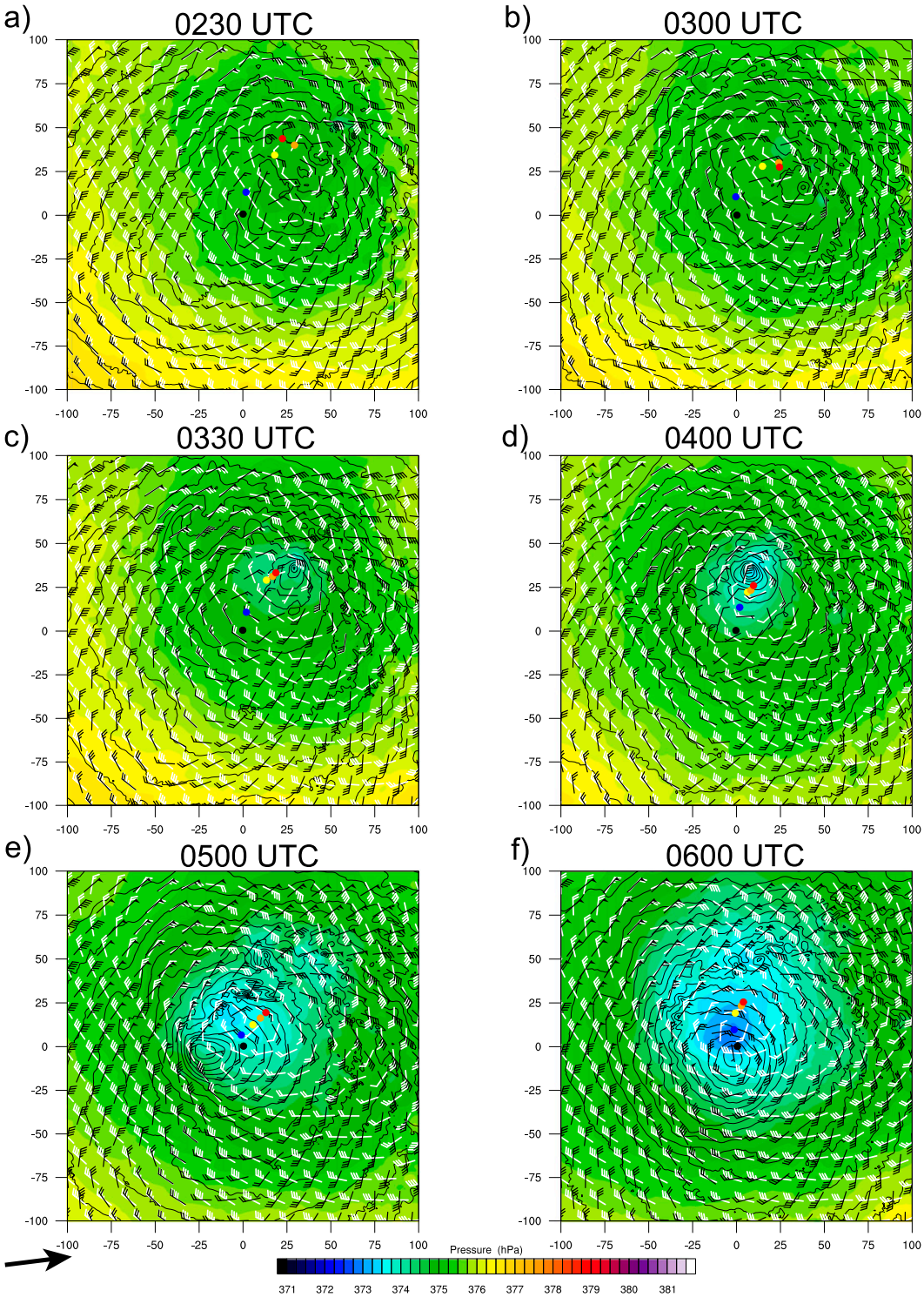

FIG. 5. Sea level pressure (contoured every 1 hPa), 8-km pressure (shaded), 10-m TC-relative wind (black barbs), and 8-km TC-relative wind (white barbs). The colored dots denote the TC center position at the surface (black), 2- (blue), 4- (yellow), 6- (orange), and 8-km (red) heights. Axis labels are in kilometers. Shear vector is denoted at bottom left.

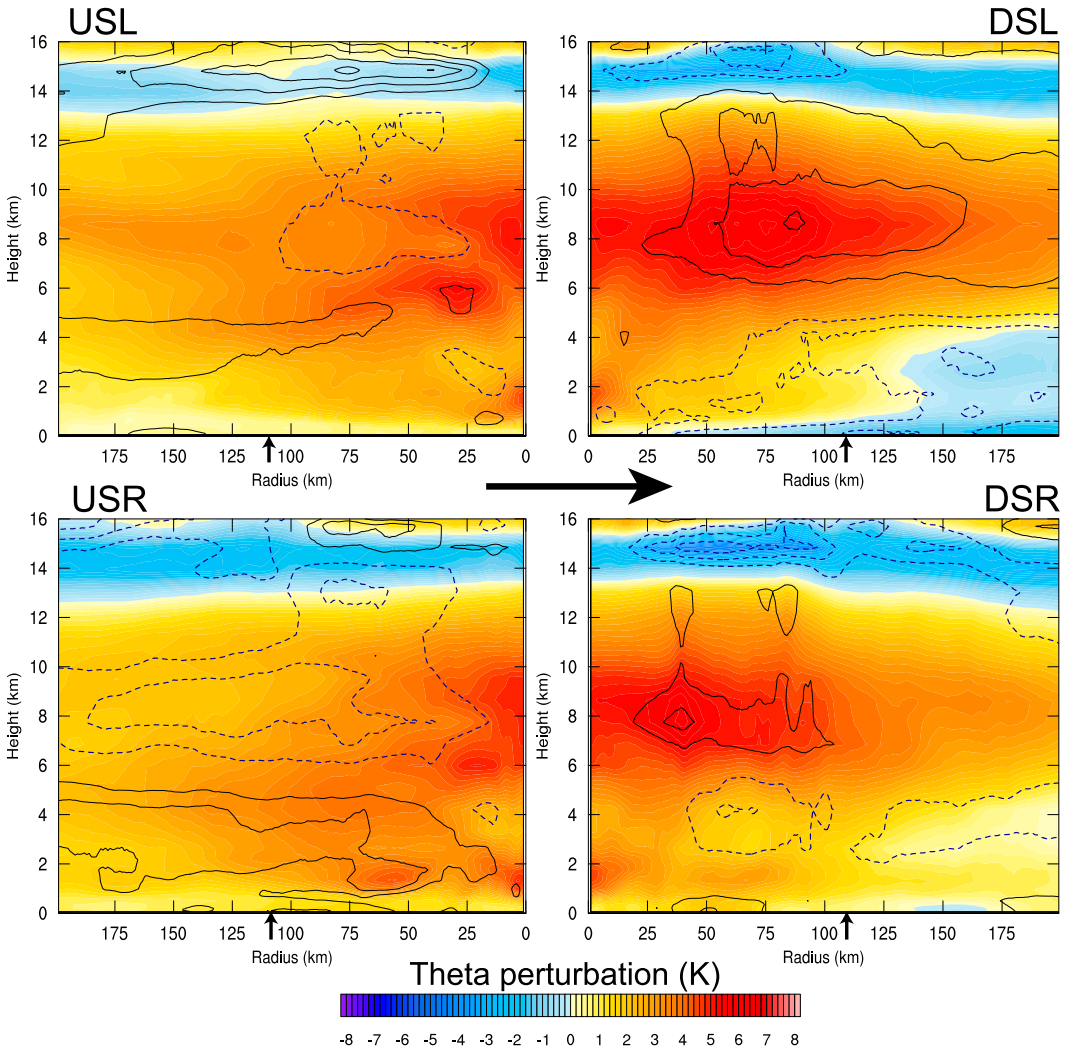

FIG. 6. Perturbation of θ from the mean at 500-km radius (shaded), positive θ perturbation from the azimuthal mean (solid black; contoured every 0.5 K starting at +0.5 K), and negative θ perturbation from the azimuthal mean (dashed blue; contoured every 0.5 K starting at −0.5 K) in each shear-relative quadrant averaged from 0200 to 0230 UTC 14 Sep. Shear vector (large arrow) points to the right. The axisymmetric RMW is indicated by the small arrows on the x axis.

respectively. As in Cram et al. (2002), the solenoidal and subgrid-scale terms were ignored, as their contributions to the vorticity tendency were found to be small in this simulation.

Figure 11 shows the time evolution of the first four terms on the right-hand side of Eq. (1) averaged within 5 km of the mesovortex center, defined by the location of maximum 1-km relative vorticity. Air converged beneath the convective updraft, resulting in extremely intense stretching of cyclonic vorticity, particularly in the lowest 1 km. Stretching reached area-averaged values of up to $100 \times 10^{-5}\,s^{-1}\,min^{-1}$ ($1.67 \times 10^{-5}\,s^{-2}$) (Fig. 11a) and instantaneous values of up to $840 \times 10^{-5}\,s^{-1}\,min^{-1}$ ($14 \times 10^{-5}\,s^{-2}$) (not shown). As noted by Haynes and McIntyre (1987), the horizontal advection term can significantly oppose the stretching term due to inflow in the presence of decreasing vorticity with radius. Near the mesovortex, anticyclonic vorticity tendencies associated with horizontal advection were observed in the lowest kilometer (Fig. 11b), although they were smaller than the cyclonic vorticity tendencies associated with stretching, suggesting the dominant role of vortex stretching in the low-level spinup of the mesovortex. To a lesser extent, tilting of horizontal vorticity into the vertical also contributed to low-level cyclonic vorticity generation in the lowest 3 km, with area-averaged values of $15–30 \times 10^{-5}\,s^{-1}\,min^{-1}$ ($0.25–0.5 \times 10^{-5}\,s^{-2}$) (Fig. 11c) and

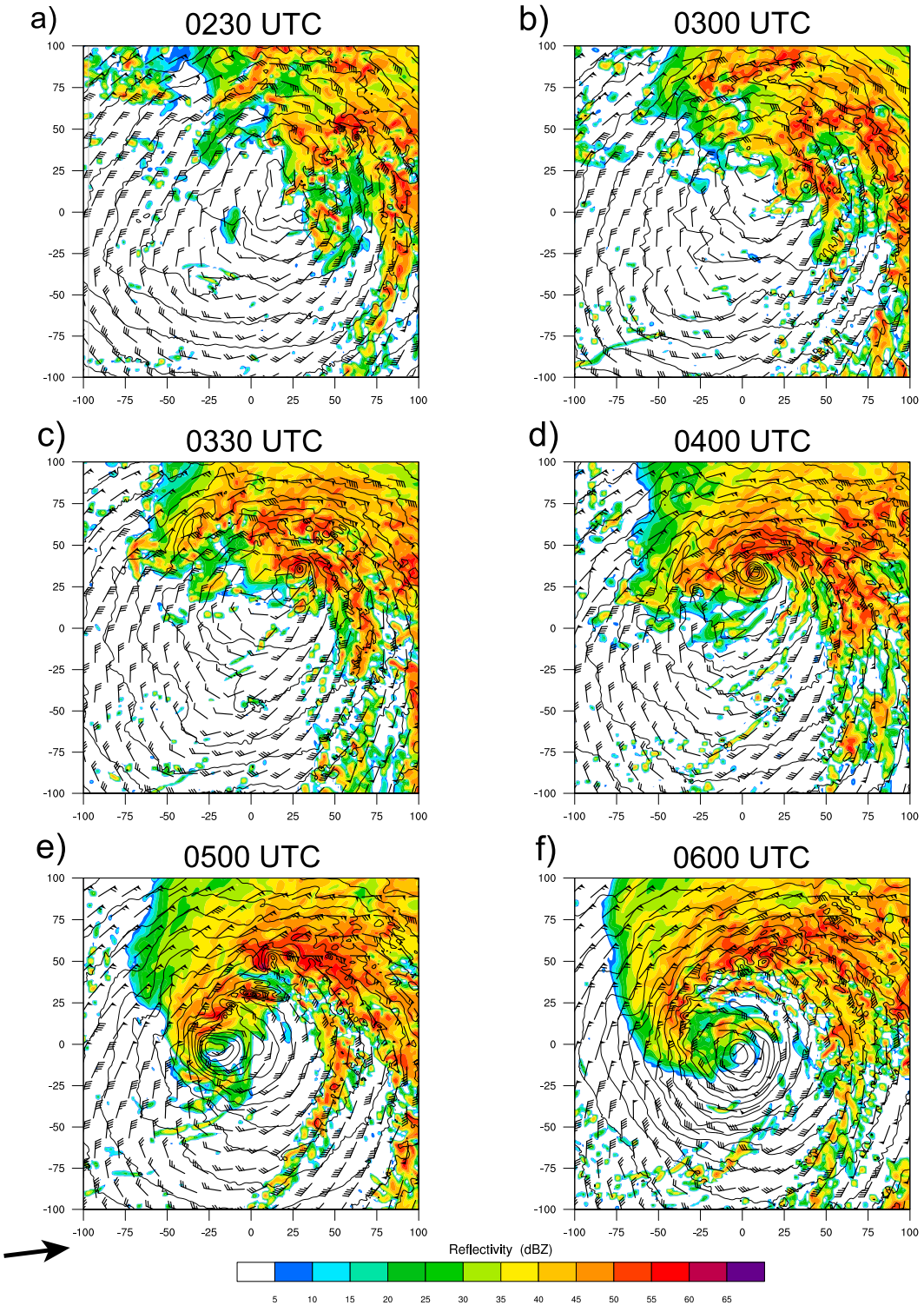

FIG. 7. Simulated reflectivity at 1-km height (shaded), sea level pressure (contoured every 1 hPa), and 10-m TC-relative winds (barbs). Axis labels are in kilometers. Shear vector is denoted at bottom left.

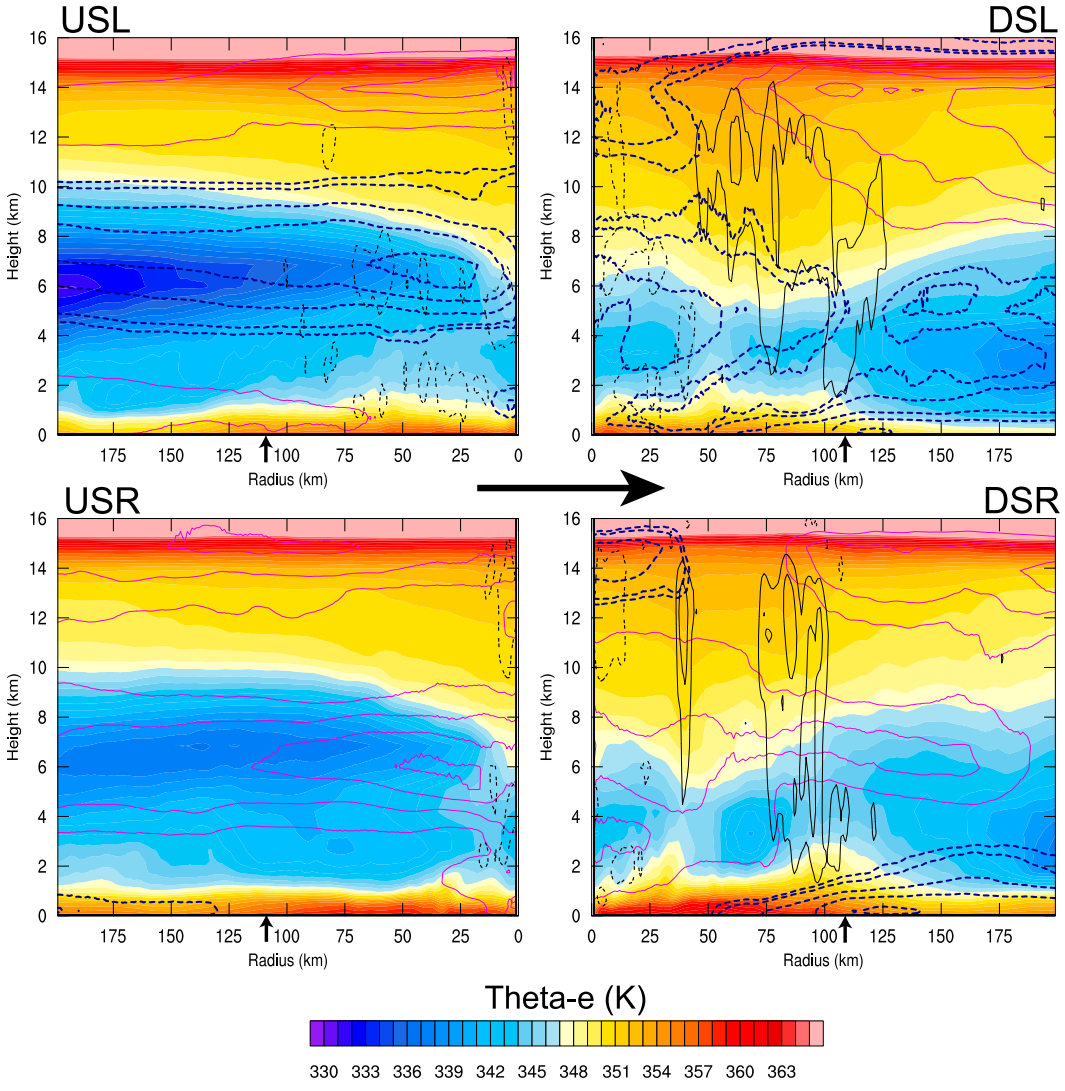

FIG. 8. θ_e (shaded), upward motion (solid black; contoured every 0.5 m s^{-1} starting at 0.5 m s^{-1}), downward motion (dashed black; contoured every 0.5 m s^{-1} starting at -0.1 m s^{-1}), TC-relative inflow (dashed blue; contoured every 3 m s^{-1} starting at -3 m s^{-1}), and TC-relative outflow (solid magenta; contoured every 3 m s^{-1} starting at 3 m s^{-1}) in each shear-relative quadrant averaged from 0200 to 0230 UTC 14 Sep. Shear vector (large arrow) points to the right. The axisymmetric RMW is indicated by the small arrows on the x axis.

instantaneous values of 180–360 $\times$ 10^{-5} s^{-1} min^{-1} (3–6 $\times$ 10^{-5} s^{-2}) (not shown). The cyclonic vorticity associated with the mesovortex expanded upward in response to the upward growth of the adjacent convective updraft (Fig. 10). This upward growth was attributed to two factors. First, vortex stretching beneath the peak of the updraft at 12-km height (Fig. 11a) overwhelmed the offsetting effects of horizontal advection (Fig. 11b). Second, although some cancellation between the tilting and vertical advection occurred, the vertical advection of vorticity by the updraft (Fig. 11d) overwhelmed the offsetting effects of tilting (Fig. 11c).

The close correspondence of the cyclonic vorticity and the convective updraft and the bottom-up intensification of the mesovortex exhibited similarities to simulations of VHTs (e.g., Hendricks et al. 2004; Montgomery et al. 2006). The intense boundary layer convergence and stretching of cyclonic vorticity shown in Fig. 11a was consistent with previous studies of VHTs in tropical cyclogenesis simulations (e.g., Nolan 2007; Fang and Zhang 2010; Wang et al. 2010). This boundary layer convergence was due to the diabatically driven secondary circulation associated with the convective updraft but may have been modified by friction. Friction has often been viewed as a contributor to spindown of the

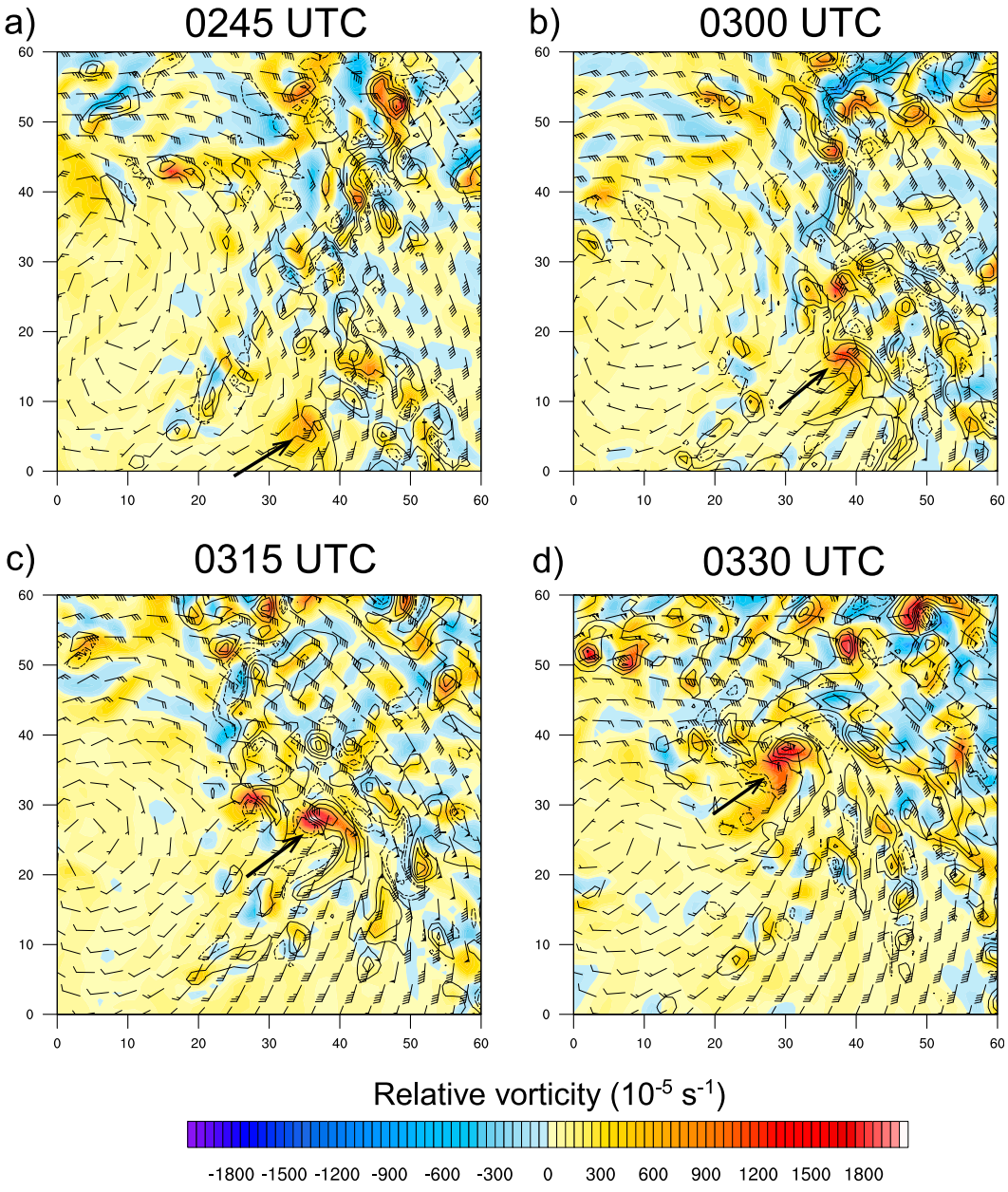

FIG. 9. Relative vorticity (shaded), TC-relative winds (barbs), upward motion (solid; contoured every 2 m s^{-1} starting at 1 m s^{-1}), and downward motion (dashed; contoured every 2 m s^{-1} starting at −1 m s^{-1}) at 1-km height. The arrow denotes the mesovortex. Axis labels are in kilometers.

vortex by reducing the near-surface flow (e.g., Raymond et al. 2007; Kepert 2011). However, Smith et al. (2009) and Montgomery and Smith (2012) hypothesize that frictional boundary layer spinup can occur if convergence of absolute angular momentum exceeds the dissipation of momentum into the underlying ocean. The contribution, if any, of friction to tropical cyclone boundary layer spinup remains a topic of further research, and the applicability of these arguments to a smaller-scale vortex (as seen in this study) remain to be seen.

6. Mesovortex evolution: Thermodynamics

The mesovortex was initially associated with a local maximum of boundary layer moist entropy. Figure 12 shows west–east cross sections of θ_e, vertical motion, and mesovortex-relative flow during the period of rapid

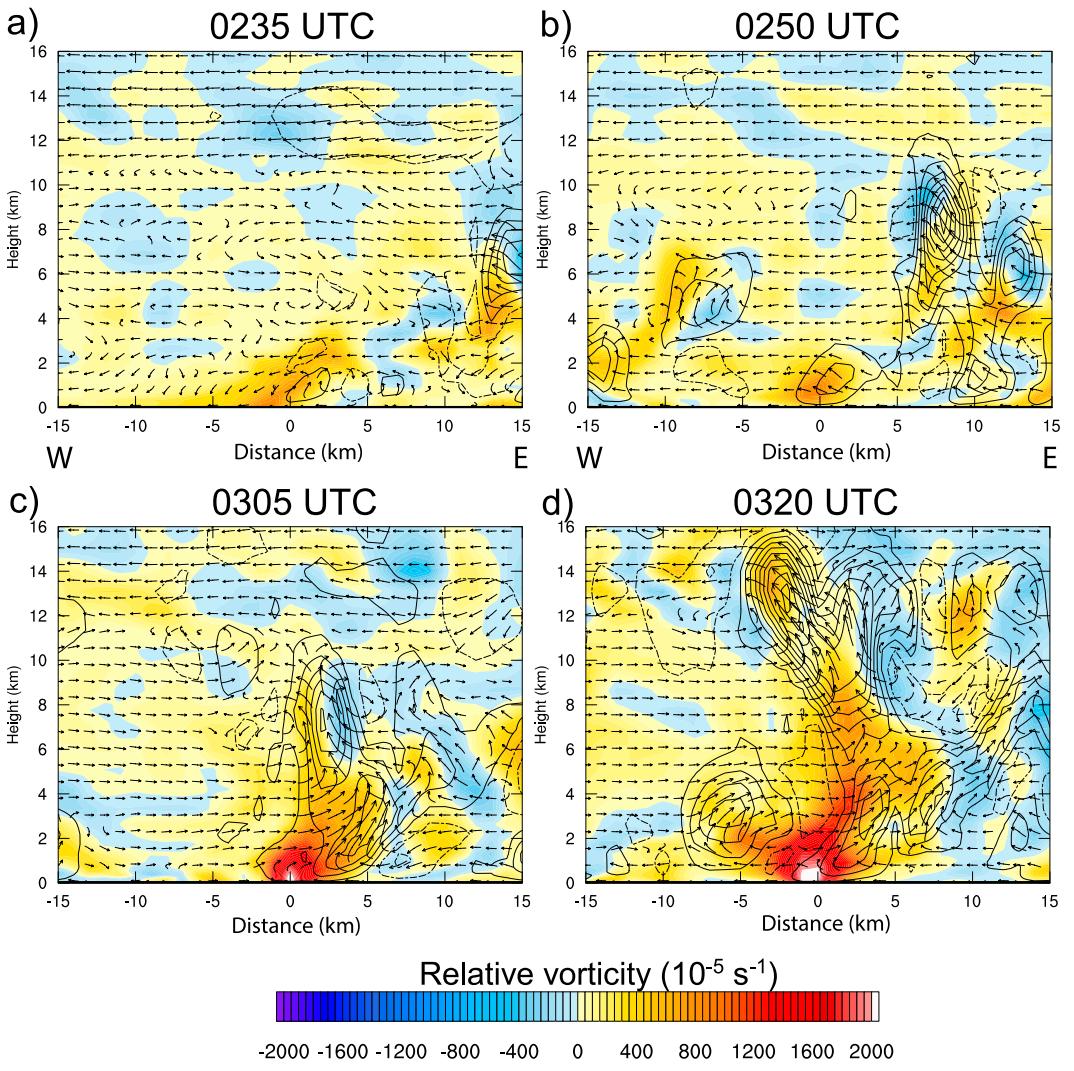

FIG. 10. West–east cross section through the mesovortex center ($x = 0$) showing relative vorticity (shaded), upward motion (solid black; contoured every 2 m s^{-1} starting at 1 m s^{-1}), downward motion (dashed blue; contoured every 2 m s^{-1} starting at −1 m s^{-1}), and mesovortex-relative flow in the west−east plane (black arrows; vertical component magnified 10 times).

spinup. At 0235 UTC 14 September, the mesovortex and adjacent updraft were quite shallow and collocated with a local maximum of near-surface θ_e near 364 K (Fig. 12a). Subsidence of 1–2 m s^{-1} was present at 2-km height and was associated with a capping inversion that stunted the updraft. Figure 13a shows a sounding taken over the mesovortex at 0235 UTC 14 September. A weak capping inversion near 2-km height overlaid the low-level saturated layer that was indicative of the shallow updraft. Fifteen minutes later, subsidence over the mesovortex dissipated, and the shallow updraft intensified and grew upward to the 3-km level (Fig. 12b). A model sounding taken over the mesovortex at this time (Fig. 13b) indicated that the capping inversion dissipated, with the temperature between 2- and 3-km height cooling about 2–3 K. The sounding was now saturated up to 3-km height, indicative of the growing updraft.

After the capping inversion dissipated, the updraft grew rapidly and reached the tropopause by 0320 UTC 14 September (Figs. 12c,d). The erosion of the capping inversion may be partially due to the thermal asymmetries associated with the tilt of the tropical cyclone vortex (Fig. 6). As the mesovortex moved toward the downtilt portion of the TC, it encountered low–potential temperature anomalies in the low to mid-troposphere. Trajectory analysis (not shown) showed that parcels ending near the mesovortex below about 1.5-km height came from upstream, while parcels ending near the mesovortex above 1.5-km height came

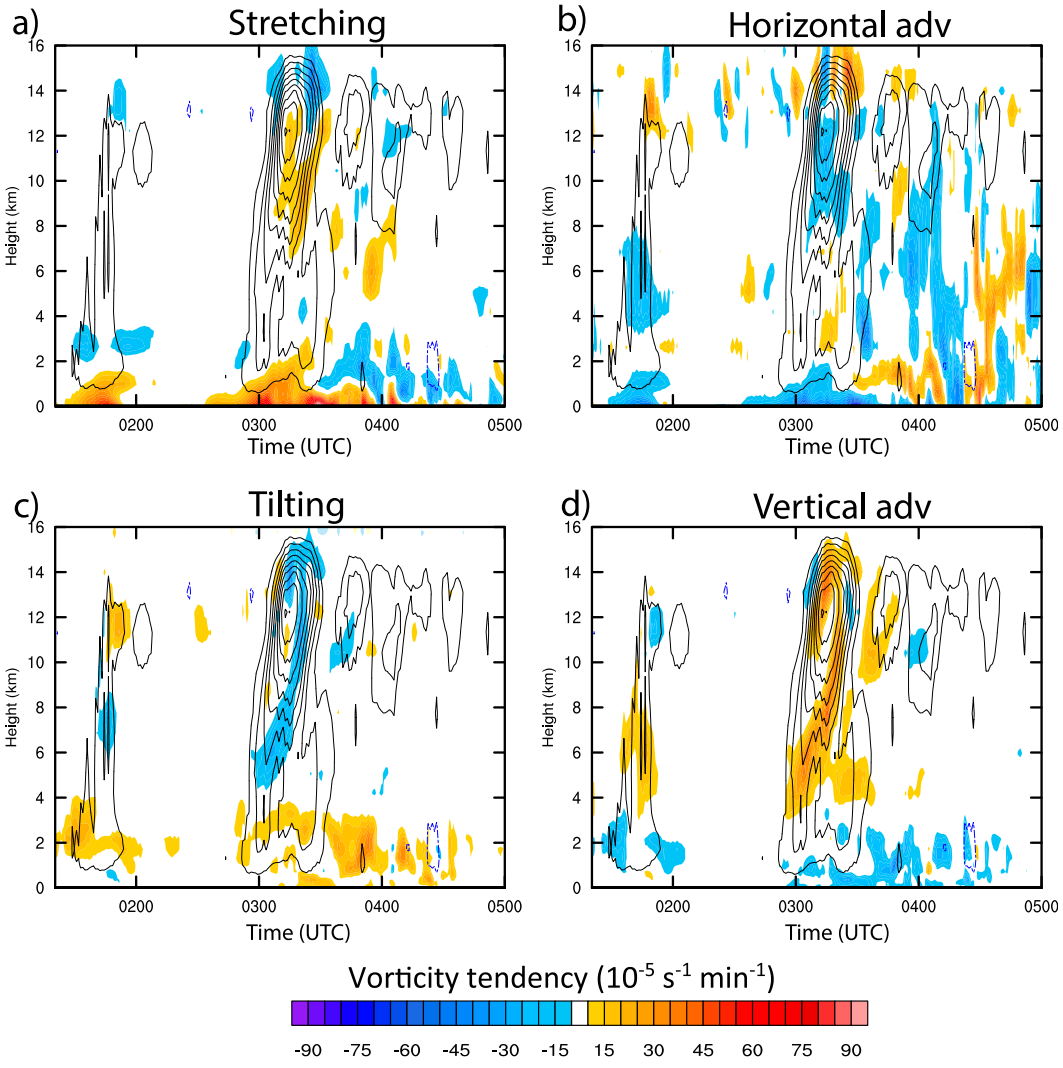

FIG. 11. Time evolution of various fields averaged within 5 km of the mesovortex center (defined as the maximum 1-km relative vorticity location). Shading denotes the contribution to the absolute vorticity tendency from (a) stretching, (b) horizontal advection, (c) tilting, and (d) vertical advection. Upward motion is shown as solid black contours (every 1 m s^{-1} starting at 1 m s^{-1}). Downward motion is shown as dashed blue contours (every 1 m s^{-1} starting at -1 m s^{-1}).

from downstream. Thus, the capping inversion was not simply advected along with the mesovortex but was continually ''recreated'' over the mesovortex by sinking air parcels that warmed dry adiabatically. When this sinking motion was replaced by ascending motion (as the mesovortex moved into the downtilt quadrant), the capping inversion eroded. A complete analysis of the erosion of the capping inversion is beyond the scope of this paper and may be worth exploring in future work.

In addition to the erosion of the capping inversion, the midtropospheric θ_e increased as the mesovortex moved into the downtilt region (Figs. 12a,b). The convective transport of boundary layer θ_e upward through the free troposphere formed a midlevel moist envelope around the midlevel TC vortex (not shown). This was evident in the enhanced midlevel θ_e downshear left (downtilt) observed in Fig. 8. This suggests weaker dry-air entrainment into the updraft, enhancing the updraft buoyancy (e.g., Romps and Kuang 2010; Molinari et al. 2012). Also, idealized simulations of convection (Raymond and Sessions 2007) and observations within pregenesis tropical disturbances (Raymond et al. 2011) suggest that cooling and moistening below the midlevel pre-TC vortex favored bottom-heavy mass flux profiles conducive for low-level vortex stretching and subsequent TC genesis. Applying this idea to a tilted TC vortex, low-to-midtropospheric cooling and enhanced

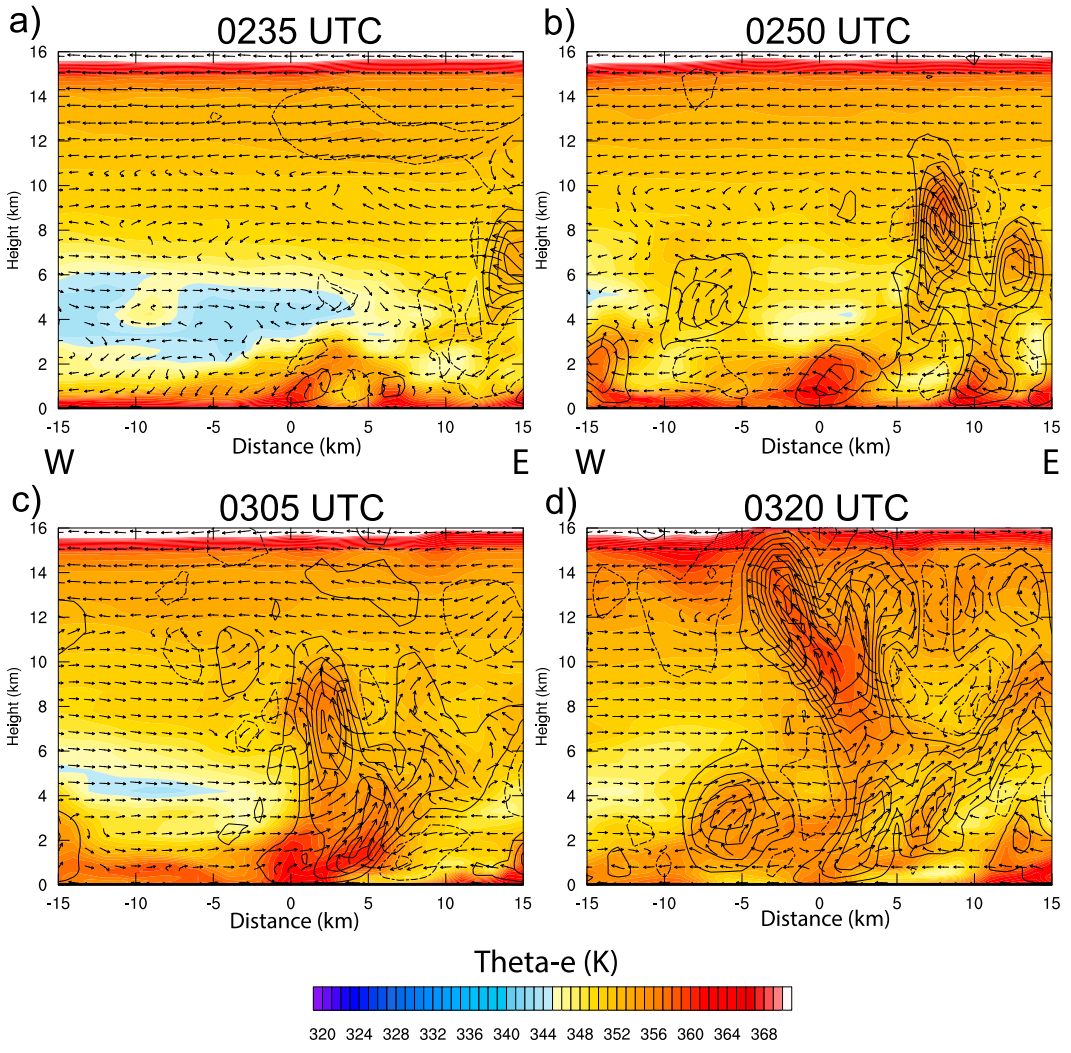

FIG. 12. As in Fig. 10, but color shading is θ_e.

midtropospheric moisture downtilt may have favored bottom-heavy vertical mass flux profiles conducive for low-level spinup of the mesovortex.

The asymmetric distribution of boundary layer moist entropy played a significant role in the development and rapid intensification of the mesovortex. Figures 14a and 14b show the distribution of θ_e at the lowest model level (~31-m height) during the early portion of the mesovortex RI. A band of high near-surface θ_e was evident in the southeastern and eastern (downshear right) portions of the tropical cyclone circulation. Because the mesovortex moved slower than the low-level flow, this high near-surface θ_e was just upstream of and fed into the mesovortex and adjacent convection. Near-surface θ_e was much lower in the northern and western quadrants (left of shear). The reasons for this asymmetry were apparent when viewing the latent heat flux and 1-km vertical motion fields. The latent heat flux field corresponded well with the strength of the surface winds, although local maxima associated with near-surface cold pools resulting from downdrafts were also observed (Figs. 14c,d). Latent heat fluxes near and upstream of the mesovortex ranged from 400 to 700 W m^{-2} and were dominant over the sensible heat fluxes, which were around 100–200 W m^{-2} (not shown). The region of highest boundary layer θ_e did not correspond well to the region of strongest latent heat fluxes. This is because boundary layer θ_e following a column of air is dependent not only on the magnitude of enthalpy fluxes from the ocean but also on mixing across the top of the boundary layer by convective downdrafts or turbulence (e.g., Anthes 1982; Dolling and Barnes 2012). Figures 14e and 14f show the vertical motion at 1-km height. The lack of low-level downdrafts upstream of the mesovortex (south and east of the TC center) suggests a lack of low-entropy intrusions

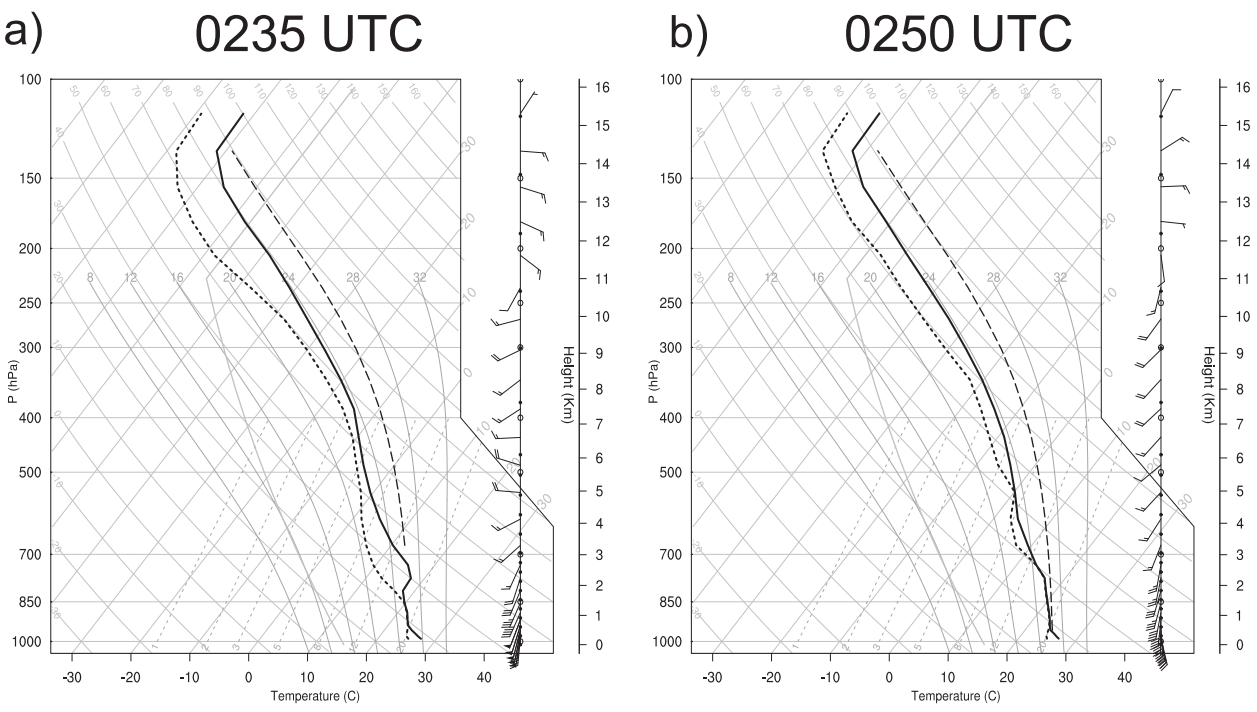

FIG. 13. Skew-*T* profiles taken at the mesovortex center at (a) 0235 UTC and (b) 0250 UTC 14 Sep.

into the boundary layer. A weak capping inversion, due to weak subsidence associated with the tilt of the TC vortex (Jones 1995), was also present over parts of the upshear and right-of-shear quadrants (not shown). This inhibited vertical mixing between the boundary layer and the air above. The lack of vertical mixing and downdraft intrusions allowed surface enthalpy fluxes to build up moist entropy in the boundary layer. This resulted in a region of convective available potential energy (CAPE) of 2000–3000 J kg^{-1} downshear to downshear right that helped fuel convection in the vicinity of the mesovortex (not shown).

A qualitatively similar thermodynamic evolution may have occurred in sheared TC Humberto (2001), as described by Dolling and Barnes (2012). In that storm, a reservoir of high low-level θ_e was observed by dropsondes upstream of downshear convection. A strong capping inversion associated with light stratiform precipitation beneath an anvil cloud, and the lack of upstream convective transports allowed θ_e to build up in the boundary layer. Dolling and Barnes (2012) hypothesized that the resulting enhanced CAPE fueled convection that was more efficient in concentrating vorticity via stretching. Although it is not known whether Humberto underwent downshear reformation owing to spatial and temporal limitations of the observations, it did intensify in a moderately sheared environment.

7. Interactions between the mesovortex, other localized cyclonic vorticity anomalies, and the TC vortex

a. Axisymmetrization

Given the marked azimuthal wavenumber-1 convective asymmetry evident in Fig. 7, and the finescale vorticity anomalies generated by downshear convective cells evident in Fig. 9, the interaction between these asymmetries and the primary TC vortex will now be explored. Many previous studies have hypothesized that axisymmetrization of convectively generated potential vorticity anomalies contributes to the intensification of the primary vortex (e.g., Montgomery and Kallenbach 1997; Möller and Montgomery 2000; Enagonio and Montgomery 2001). Although the mesovortex was the most persistent and intense cyclonic vorticity anomaly, it was one of many vorticity anomalies, both cyclonic and anticyclonic (Fig. 9). To assess the aggregate effect of the convectively generated vorticity anomalies downtilt, the 1-km relative vorticity was averaged within 25 km of each grid point (Figs. 15a–c). This is analogous to the circulation about a circle of 25-km radius centered on each grid point following Stokes's theorem. This field was very similar to both the smoothed vorticity field (not shown) and the sea level pressure field (Figs. 5 and 6).

Prior to the development of the mesovortex (Fig. 15a), a broad region of cyclonic circulation was evident,

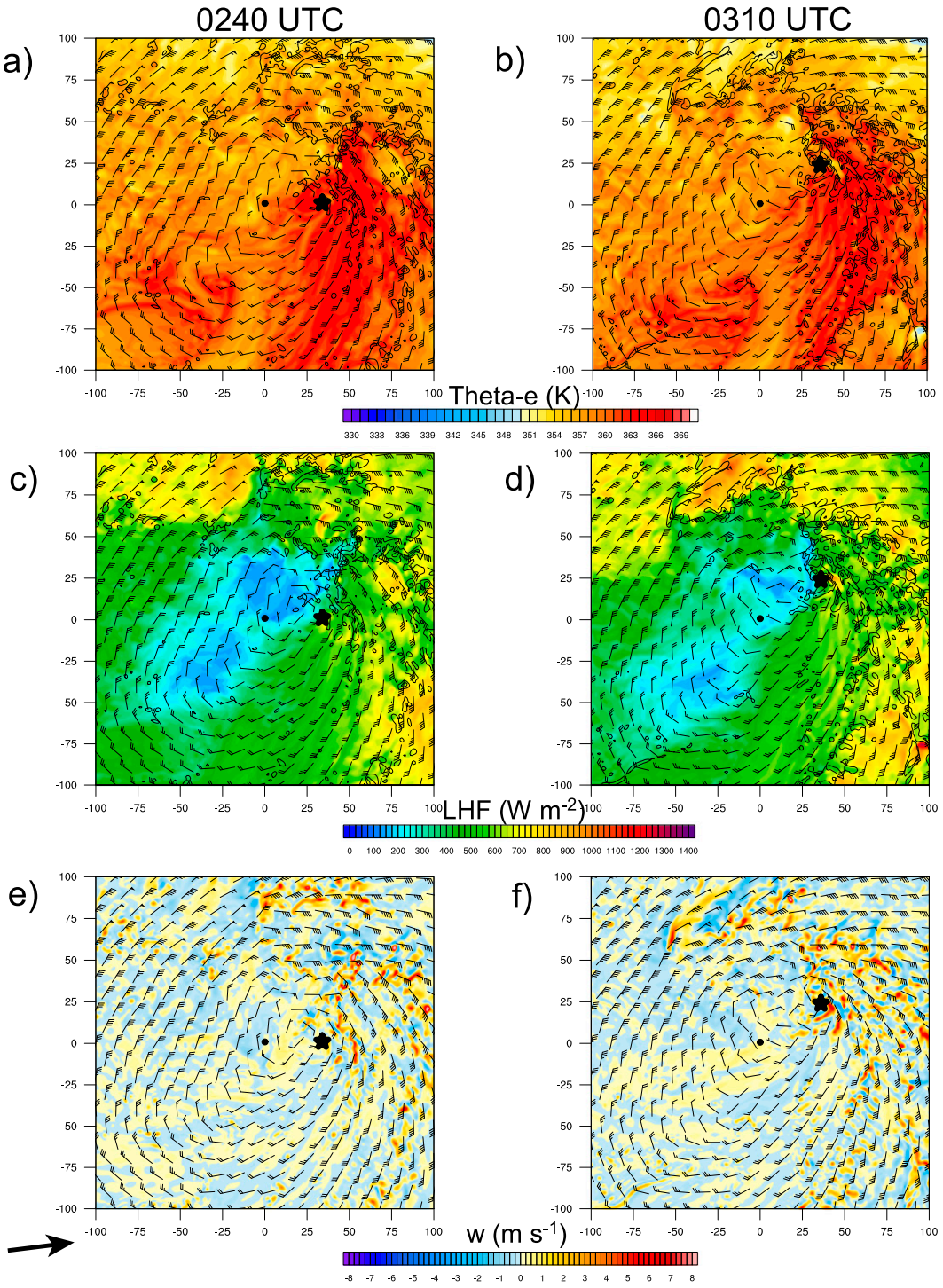

FIG. 14. (a),(b) θ_e at 31-m height (shaded), 1-km upward motion (solid; contoured every 4 m s^{-1} starting at 1 m s^{-1}), 1-km downward motion (dashed; contoured every 4 m s^{-1} starting at -1 m s^{-1}), and TC-relative 10-m winds (barbs); (c),(d) latent heat flux (shaded), 1-km upward motion (solid; contoured every 4 m s^{-1} starting at 1 m s^{-1}), 1-km downward motion (dashed; contoured every 4 m s^{-1} starting at -1 m s^{-1}), and TC-relative 10-m winds (barbs); (e),(f) 1-km vertical motion (shaded) and TC-relative 10-m winds (barbs). The black dot denotes the TC center at the surface. The star denotes the mesovortex location. Axis labels are in kilometers. Shear vector is shown at bottom left.

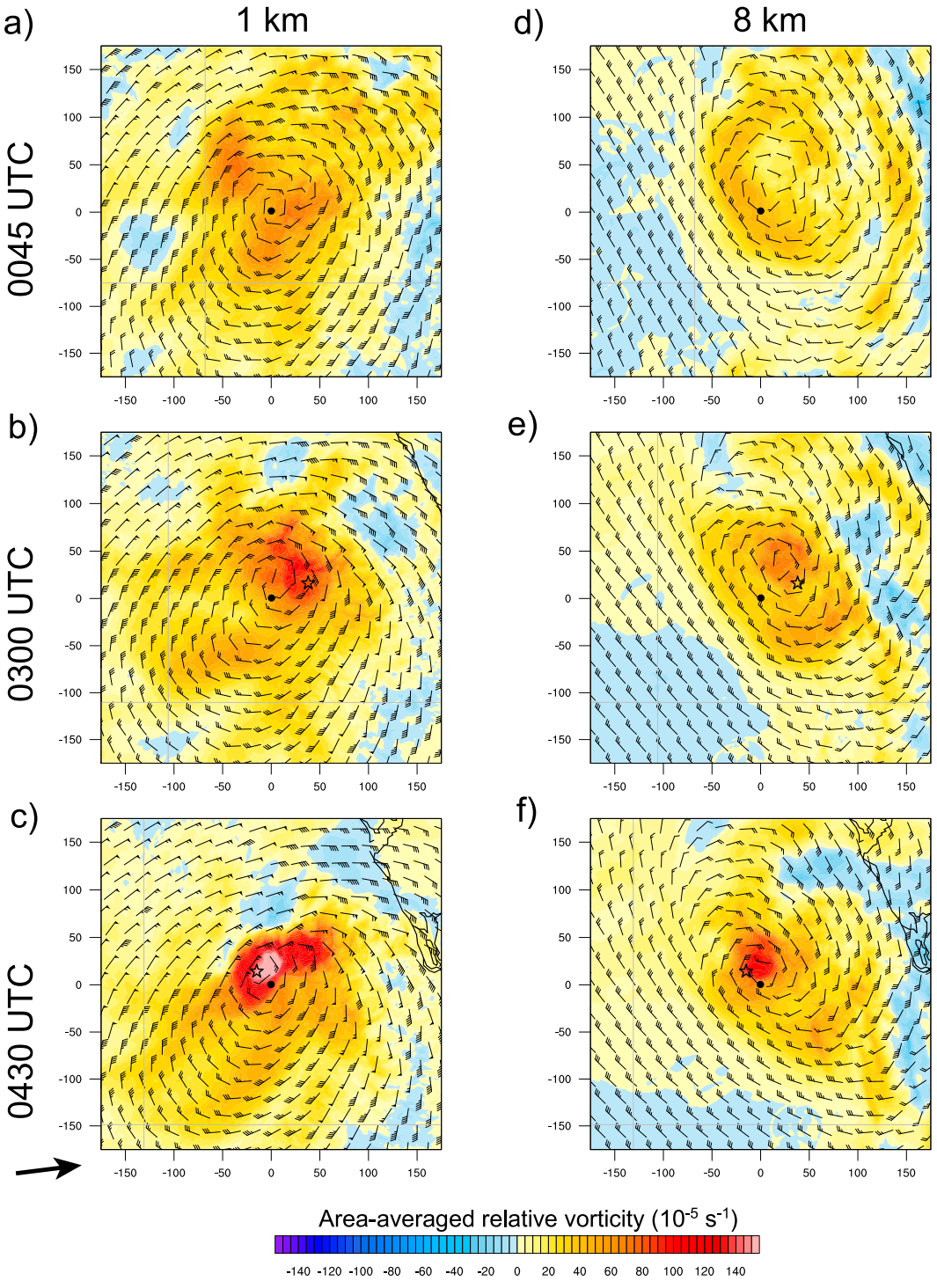

FIG. 15. Relative vorticity averaged within 25 km of each grid point (color shading) and TC-relative winds at (a)–(c) 1- and (d)–(f) 8-km height. The black dot denotes the TC center at the surface. The star denotes the mesovortex location. Axis labels are in kilometers. Shear vector is shown at bottom left.

reflective of the initial TC vortex (parent vortex). By 0300 UTC 14 September (Fig. 15b), cyclonic circulation increased markedly in the vicinity of downshear convection northeast of the low-level TC center. The increase in cyclonic circulation confirmed the dominance of the cyclonic vorticity anomalies over the anticyclonic vorticity anomalies seen in Fig. 9. This local region of enhanced cyclonic circulation comprised an

"inner vortex" embedded in the broad envelope of cyclonic circulation associated with the parent vortex. The inner vortex became the dominant vortex, with its cyclonic flow advecting and axisymmetrizing the parent vortex. Note that the broad envelope of cyclonic circulation to the southwest of the inner vortex at 0300 UTC (Fig. 15b) rotated to the southern and southeastern sides of the inner vortex by 0430 UTC (Fig. 15c). The region of weak anticyclonic circulation to the east-northeast of the inner vortex at 0300 UTC (Fig. 15b) rotated to the northern side of the inner vortex by 0430 UTC (Fig. 15c). This evolution was also apparent in the sea level pressure field evolution shown in Fig. 7. As the inner vortex initially formed (Fig. 7a), the parent vortex was on its western flank. As the inner vortex rapidly intensified, the parent vortex was advected to the southwestern (Figs. 7b,c), southern (Fig. 7d), and eastern (Fig. 7e) flanks of the inner vortex. By 0600 UTC 14 September, the inner vortex had completely absorbed the parent vortex, and the convective structure became more axisymmetric as convection was able to wrap around to the northwestern quadrant (Fig. 7f).

This evolution resembled the simulations done by Enagonio and Montgomery (2001, hereafter EM01). Using a shallow-water primitive equation model, EM01 investigated the impact of asymmetric, convectively generated vorticity anomalies on the intensification of the parent vortex. One set of simulations involved the interaction of two vortices: an intense, small-scale vortex embedded within a broad, weaker parent vortex at the tropical cyclogenesis stage. The smaller intense vortex was placed at the radius of maximum winds of the parent vortex. In these simulations, the small vortex became the dominant vortex, acting to distort and advect the parent vortex until the system became nearly axisymmetric (see Fig. 12 in EM01). Although there are similarities between the evolution in EM01's simulations and the current Gabrielle simulation, there existed several differences. The Gabrielle simulation was a full-physics simulation, whereas EM01 utilized a shallow-water primitive equation model that did not simulate active convection. The ambient vertical wind shear in the Gabrielle simulation continuously forced an azimuthal wavenumber-1 convective asymmetry, whereas the forcing was prescribed at one time and was not continuous in the EM01 simulations. The shear also acted to tilt the parent vortex in the Gabrielle simulation. Because of the continuous forcing by ambient vertical wind shear, the TC in the Gabrielle simulation was never able to become completely axisymmetric as in the EM01 simulations. Also, the Gabrielle inner vortex did not comprise a single cyclonic vorticity maximum initialized in the EM01 simulation. However, collectively the cyclonic vorticity maxima would behave similarly to the single cyclonic vorticity anomaly initialized in EM01 through their circulation following Stokes's theorem. Finally, the Gabrielle parent vortex was stronger (15–20 $m\,s^{-1}$) than the parent vortex used by EM01 (5 $m\,s^{-1}$). The impact of the strength of the parent vortex on the likelihood of downshear reformation will be speculated upon in the discussion section.

b. *Reduction of vortex tilt*

The development of the inner vortex and subsequent axisymmetrization process may have helped the TC vortex resist the shear. Prior to the development of the inner vortex, tilt of the parent vortex was evident by the displacement of the 8-km circulation envelope (Fig. 15d) to the northeast (downshear left) of the 1-km circulation envelope (Fig. 15a). By 0300 UTC 14 September, the inner vortex developed and was nearly upright. Note that the maximum circulation at 1-km height (Fig. 15b) and the maximum circulation at 8-km height (Fig. 15e) were nearly collocated. By 0430 UTC 14 September, the circulation associated with the inner vortex intensified at both 1- and 8-km heights (Figs. 15c,f). The inner vortex remained nearly vertically aligned, while the downshear-left tilt of the parent vortex persisted. The much larger tilt of the parent, outer vortex in comparison to the tilt of the inner vortex has been noted in other simulations of tropical cyclones in shear, both in dry (e.g., Jones 1995; Reasor et al. 2004) and in full-physics (e.g., Riemer et al. 2010) simulations. However, in the current simulation, the inner vortex appears to have been a new feature that formed as a result of downshear convection. This differed from the inner vortex that was prescribed initially in the dry simulations (e.g., Jones 1995; Reasor et al. 2004) and the already-established inner vortex of the mature TC simulated in the full-physics simulation of Riemer et al. (2010). Once the inner vortex was established, the nearly upright inner, tilted outer vortex tilt structure persisted another 6 h until landfall (not shown). Reasor et al. (2004) noted that their spatially nonuniform tilt was the result of the emerging quasi mode, consistent with their vortex Rossby wave theory for vortex resilience. The reduced static stability in the vicinity of moist convection may have also played a role by enhancing vertical coupling between the upper and lower PV anomalies (e.g., Jones 1995; Reasor et al. 2004), enabling the inner vortex to remain upright.

Figure 16 shows the time evolution of the surface-to-8-km TC vortex tilt. The TC vortex tilt was initially about 65 km prior to the development of the inner vortex. At this time, the TC vortex tilt measured the tilt of the broad cyclonic circulation associated with the

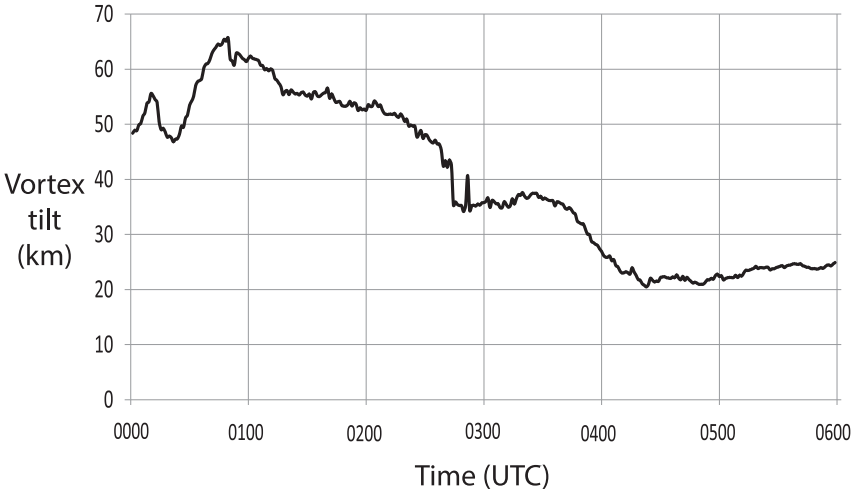

FIG. 16. TC vortex-tilt magnitude between the surface and 8-km height.

parent vortex (Figs. 15a,d). As the upright inner vortex developed and became the dominant vortex in the system, the TC vortex tilt became increasingly representative of the inner vortex tilt instead of the parent vortex tilt. Also, the cyclonic propagation of the mesovortex, the spinup of the mesovortex, and the spinup of adjacent cyclonic vorticity anomalies helped increase the low-level circulation downtilt and beneath the upper portion of the TC vortex. This resulted in a reduction of TC vortex tilt to near 20 km by 0430 UTC 14 September. The reduction of TC vortex tilt during the downshear reformation process was also observed in a high-resolution WRF simulation of Irene (2005) (Davis et al. 2008, their Fig. 3). In their simulation, the TC vortex tilt decreased from about 90 to 20 km in 6 h as a new vortex formed downshear. Thus, the formation of an upright inner vortex could be one way that diabatic heating associated with downshear convection can help tropical cyclones withstand environmental vertical wind shear.

8. Discussion

Tropical Storm Gabrielle (2001) experienced a 22-hPa surface pressure fall in less than 3 h while undergoing environmental vertical wind shear of 12–13 $m\,s^{-1}$. A new vortex within downshear convection formed during this short-term rapid intensification event, as confirmed by aircraft reconnaissance and land-based radar observations (Molinari and Vollaro 2010). A 1-km-horizontal-resolution WRF simulation of this event was used to explore in detail the downshear reformation process and gain better understanding of how tropical cyclones interact with environmental vertical wind shear.

Figure 17 shows a schematic diagram of the relevant processes involved in downshear reformation. The environmental shear tilted the parent TC vortex downshear left (Fig. 5) and forced azimuthal wavenumber-1 kinematic and thermodynamic asymmetries. Enhanced low-level inflow and convergence were observed in the downshear quadrants (Fig. 8). The enhanced low-level convergence and lifting helped initiate convection preferentially downshear and downshear right (Fig. 7). As convection matured downshear left, downdrafts enhanced by evaporation and water loading deposited low-entropy air into the boundary layer (Fig. 8). As this entropy-depleted boundary layer air was advected through the upshear and right of shear quadrants, the combination of surface enthalpy fluxes and a lack of penetrative downdrafts (Fig. 14) allowed moist entropy to increase to a maximum downshear right. This enhanced boundary layer moist entropy combined with low-to-midtropospheric cooling downtilt contributed to a region of more than 2000 $J\,kg^{-1}$ of CAPE that fueled the downshear convection.

These TC vortex-scale kinematic and thermodynamic asymmetries resulted in a favorable local environment for sustained, intense convection downshear. Many localized convective cells with adjacent cyclonic vorticity cores developed downshear, including one particularly intense mesovortex. Initially, this mesovortex was quite shallow with cyclonic vorticity mostly confined to the lowest 2 km (Figs. 10a,b). This was due to the presence of a capping inversion (Fig. 13a), which limited the vertical extent of the convective updraft. However, as the local mesovortex environment cooled in the low to midtroposphere, the inversion dissipated (Fig. 13b), and the convective updraft grew explosively upward (Figs. 10c,d). Maximum relative vorticity in the boundary layer tripled to $2.2 \times 10^{-2}\,s^{-1}$ in a span of 25 min. Convergence and stretching of cyclonic vorticity played a

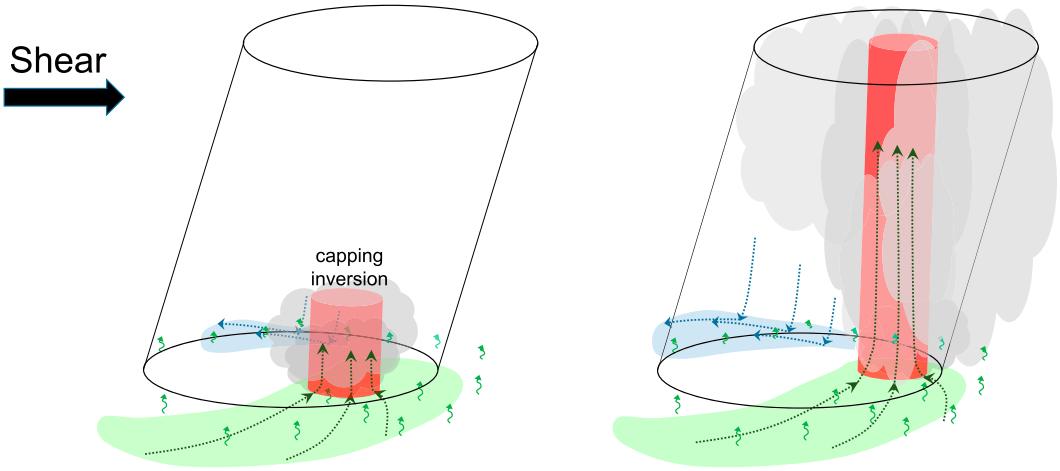

FIG. 17. Three-dimensional schematic diagram summarizing the downshear reformation of Tropical Storm Gabrielle. The red cylinder represents the inner vortex at (a) early stages and (b) the mature stage, when it has become the dominant vortex of the storm. The larger tilted cylinder represents the broad parent vortex. Gray clouds denote the downshear convection. The green- and blue-shaded regions indicate, respectively, the enhanced boundary layer θ_e downshear right and depleted boundary layer θ_e left of shear. Dark green arrows represent boundary layer convergence and upward motion in the vicinity of the inner vortex. Blue arrows denote downdrafts and boundary layer divergence left of shear. Light green wavy arrows denote surface enthalpy fluxes.

key role in the boundary layer spinup of the mesovortex (Fig. 11b), dominating the partially offsetting effects of horizontal advection (Fig. 11c). Cyclonic vorticity remained maximized in the boundary layer and intensified upward with the growth of the convective plume (Figs. 10 and 11a). The upward growth of cyclonic vorticity was attributed to both vortex stretching beneath the peak vertical velocity of the convective updraft and vertical advection of vorticity by the convective updraft (Fig. 11e).

This mesovortex was the most sustained and intense of many cyclonic vorticity anomalies that developed within the downshear convection. Collectively, these cyclonic vorticity anomalies helped increase the low-level circulation beneath the upper portion of the tilted parent (outer) vortex. This increase in circulation constituted a newly developed "inner vortex" that was nearly upright. This inner vortex became the dominant vortex of the system, advecting and then absorbing the broad, tilted parent vortex. The reduction of TC vortex tilt from 65 to 20 km in 3 h (Fig. 16) reflected the emerging dominance of this upright inner vortex. A similar decrease in TC vortex tilt during downshear reformation was observed by Davis et al. (2008) in their simulation of TC Irene (2005). Airborne Doppler radar observations of TC Earl (2010) also showed a decrease in TC vortex tilt associated with a downtilt convective burst (Rogers et al. 2015). The development of a new, upright vortex within downtilt convection may have played a key role in decreasing the TC vortex tilt in each of these cases. The relocation of the TC center closer to the convection would also have enabled more diabatic heating to occur closer to the TC center. Diabatic heating within the high-inertial-stability region inside the radius of maximum wind was found to be particularly important for TC intensification, both in balanced vortex models (e.g., Pendergrass and Willoughby 2009; Vigh and Schubert 2009) and in observations (e.g., Rogers et al. 2013). Thus, we hypothesize that downshear reformation, resulting from diabatic heating associated with asymmetric convection, can help the TC resist shear by reducing vortex tilt (via the formation of a new, upright vortex) and by enhancing the conversion of heating into kinetic energy (Nolan et al. 2007).

The evolution described above raises the still-unresolved question: why do not all sheared storms undergo the downshear reformation process? The hypothesized negative impacts of environmental vertical wind shear, including midtropospheric ventilation (Simpson and Riehl 1958; Tang and Emanuel 2010), upper-tropospheric ventilation (Frank and Ritchie 2001), and excitation of lower-tropospheric downdrafts (Riemer et al. 2010), may act to prevent downshear reformation from occurring. Although downshear convection in asymmetric tropical cyclones can help spin up a new vortex and aid the TC in resisting the shear, convective downdrafts can have a detrimental effect. Lower-tropospheric downdrafts observed in sheared Tropical Storm Edouard (2002) lowered the boundary layer θ_e by 4–6 K and shut down subsequent convection

for about 12 h (Molinari et al. 2013). Extremely dry midtropospheric air was present in the vicinity of Edouard, which enhanced the downdraft convective available potential energy and likely contributed to the intensity of the downdrafts. In idealized convection-permitting simulations conducted by Rappin et al. (2010), larger midlevel saturation deficits resulted in enhanced downdrafts that disrupted the formation of a new vortex downshear, preventing intensification and the development of a vertically stacked vortex. Low-level divergence associated with lower-tropospheric downdrafts would also lead to vortex compression, interrupting the formation of a new vortex. Thus, we speculate that TCs that undergo downshear reformation may have less downdraft activity, possibly because of a moister environment. Indeed, Tropical Storm Edouard (2002) did not appear to undergo downshear reformation. How downdrafts and other negative influences of environmental vertical wind shear affect the TC's attempts to resist shear through downshear reformation remains a subject for future study.

The downshear-reformation cases that have been documented thus far in observations (Molinari et al. 2004; Molinari and Vollaro 2010) and models (Davis et al. 2008) have occurred when the TC was at tropical storm intensity. In the aforementioned EM01 study, the extent to which the new vortex established itself as the dominant vortex of the system depended on its intensity relative to the parent vortex. This suggests that downshear reformation would be more likely to occur when the parent vortex is relatively weak (i.e., tropical depressions and tropical storms) and more able to be distorted and absorbed by the new vortex. In more intense TCs, development of a new vortex would be interrupted as a result of rapid axisymmetrization by the intense radial shear of the tangential flow associated with the parent vortex.

The rapid spinup and small size of the new vortex make downshear reformation difficult to observe in nature, given the spatial and temporal constraints of aircraft reconnaissance, satellite, and radar observations. As a result, downshear reformation may be a more common occurrence than is currently realized, particularly in weaker TCs. More observations in the downshear convective region of weaker TCs would be informative. Given observational constraints, ensembles of convection-permitting simulations of sheared TCs could be used to explore how often downshear reformation might occur in nature and to what extent it helps the TC resist shear. Better understanding of this process would likely improve intensity forecasts of sheared tropical cyclones.

Acknowledgments. We thank Ryan Torn of our department for his suggestions regarding the model setup and choice of model physics. We thank the three anonymous reviewers for their thorough and insightful comments. This work was supported by NSF Grants ATM AGS1132576 and ATM AGS1453311.

REFERENCES

Anthes, R. A., Ed., 1982: *Tropical Cyclones: Their Evolution, Structure and Effects*. *Meteor. Monogr.*, No. 41, Amer. Meteor. Soc., 208 pp.

Bell, M. M., and M. T. Montgomery, 2010: Sheared deep vortical convection in pre-depression Hagupit during TCS08. *Geophys. Res. Lett.*, **37**, L06802, doi:10.1029/2009GL042313.

Braun, S. A., M. T. Montgomery, and Z. Pu, 2006: High-resolution simulation of Hurricane Bonnie (1998). Part I: The organization of eyewall vertical motion. *J. Atmos. Sci.*, **63**, 19–42, doi:10.1175/JAS3598.1.

Chen, S. S., J. A. Knaff, and F. D. Marks, 2006: Effects of vertical wind shear and storm motion on tropical cyclone rainfall asymmetries deduced from TRMM. *Mon. Wea. Rev.*, **134**, 3190–3208, doi:10.1175/MWR3245.1.

Corbosiero, K. L., and J. Molinari, 2002: The effect of vertical wind shear on the distribution of convection in tropical cyclones. *Mon. Wea. Rev.*, **130**, 2110–2132, doi:10.1175/1520-0493(2002)130<2110:TEOVWS>2.0.CO;2.

Cram, T. A., M. T. Montgomery, and R. F. A. Hertenstein, 2002: Early evolution of vertical vorticity in a numerically simulated idealized convective line. *J. Atmos. Sci.*, **59**, 2113–2127, doi:10.1175/1520-0469(2002)059<2113:EEOVVI>2.0.CO;2.

Davis, C. A., S. C. Jones, and M. Riemer, 2008: Hurricane vortex dynamics during Atlantic extratropical transition. *J. Atmos. Sci.*, **65**, 714–736, doi:10.1175/2007JAS2488.1.

DeHart, J. C., R. A. Houze Jr., and R. F. Rogers, 2014: Quadrant distribution of tropical cyclone inner-core kinematics in relation to environmental shear. *J. Atmos. Sci.*, **71**, 2713–2732, doi:10.1175/JAS-D-13-0298.1.

DeMaria, M., 2010: Tropical cyclone intensity change predictability estimates using a statistical-dynamical model. *29th Conf. on Hurricanes and Tropical Meteorology*, Tuscon, AZ, Amer. Meteor. Soc., 9C.5. [Available online at http://ams.confex.com/ams/29Hurricanes/techprogram/paper_167916.htm.]

——, C. R. Sampson, J. A. Knaff, and K. D. Musgrave, 2014: Is tropical cyclone intensity guidance improving? *Bull. Amer. Meteor. Soc.*, **95**, 387–398, doi:10.1175/BAMS-D-12-00240.1.

Dolling, K. P., and G. M. Barnes, 2012: The creation of a high equivalent potential temperature reservoir in Tropical Storm Humberto (2001) and its possible role in storm deepening. *Mon. Wea. Rev.*, **140**, 492–505, doi:10.1175/MWR-D-11-00068.1.

Dudhia, J., 1989: Numerical study of convection observed during the winter monsoon experiment using a mesoscale two-dimensional model. *J. Atmos. Sci.*, **46**, 3077–3107, doi:10.1175/1520-0469(1989)046<3077:NSOCOD>2.0.CO;2.

Enagonio, J., and M. T. Montgomery, 2001: Tropical cyclogenesis via convectively forced vortex Rossby waves in a shallow water primitive equation model. *J. Atmos. Sci.*, **58**, 685–705, doi:10.1175/1520-0469(2001)058<0685:TCVCFV>2.0.CO;2.

Fang, J., and F. Zhang, 2010: Initial development and genesis of Hurricane Dolly (2008). *J. Atmos. Sci.*, **67**, 655–672, doi:10.1175/2009JAS3115.1.

Frank, W. M., and E. A. Ritchie, 1999: Effects of environmental flow upon tropical cyclone structure. *Mon. Wea. Rev.*, **127**, 2044–2061, doi:10.1175/1520-0493(1999)127<2044:EOEFUT>2.0.CO;2.

——, and ——, 2001: Effects of vertical wind shear on the intensity and structure of numerically simulated hurricanes. *Mon. Wea. Rev.*, **129**, 2249–2269, doi:10.1175/1520-0493(2001)129<2249:EOVWSO>2.0.CO;2.

Haynes, P. H., and M. E. McIntyre, 1987: On the evolution of vorticity and potential vorticity in the presence of diabatic heating and frictional or other forces. *J. Atmos. Sci.*, **44**, 828–841, doi:10.1175/1520-0469(1987)044<0828:OTEOVA>2.0.CO;2.

Hendricks, E. A., M. T. Montgomery, and C. A. Davis, 2004: The role of "vortical" hot towers in the formation of Tropical Cyclone Diana (1984). *J. Atmos. Sci.*, **61**, 1209–1232, doi:10.1175/1520-0469(2004)061<1209:TROVHT>2.0.CO;2.

Hong, Y.-Y., and J.-O. J. Lim, 2006: The WRF single-moment 6-class microphysics scheme (WSM6). *J. Korean Meteor. Soc.*, **42**, 129–151.

Houze, R. A., Jr., W.-C. Lee, and M. M. Bell, 2009: Convective contribution to the genesis of Hurricane Ophelia (2005). *Mon. Wea. Rev.*, **137**, 2778–2800, doi:10.1175/2009MWR2727.1.

Jones, S. C., 1995: The evolution of vortices in vertical shear. I: Initially barotropic vortices. *Quart. J. Roy. Meteor. Soc.*, **121**, 821–851, doi:10.1002/qj.49712152406.

——, 2000: The evolution of vortices in vertical shear. III: Baroclinic vortices. *Quart. J. Roy. Meteor. Soc.*, **126**, 3161–3185, doi:10.1002/qj.49712657009.

Kain, J. S., and J. M. Fritsch, 1993: Convective parameterization for mesoscale models: The Kain–Fritcsh scheme. *The Representation of Cumulus Convection in Numerical Models*, *Meteor. Monogr.*, No. 46, Amer. Meteor. Soc., 165–170.

Kaplan, J., M. DeMaria, and J. A. Knaff, 2010: A revised tropical cyclone rapid intensification index for the Atlantic and eastern North Pacific basins. *Wea. Forecasting*, **25**, 220–241, doi:10.1175/2009WAF2222280.1.

Kepert, J. D., 2011: Tropical cyclone structure and dynamics. *Global Perspectives on Tropical Cyclones: From Science to Mitigation*, J. C. L. Chan and J. D. Kepert, Eds., World Scientific Series on Asia-Pacific Weather and Climate, Vol. 4, World Scientific, 448 pp.

Kilroy, G., and R. K. Smith, 2013: A numerical study of rotating convection during tropical cyclogenesis. *Quart. J. Roy. Meteor. Soc.*, **139**, 1255–1269, doi:10.1002/qj.2022.

——, ——, and U. Wissmeier, 2014: Tropical convection: The effects of ambient vertical and horizontal vorticity. *Quart. J. Roy. Meteor. Soc.*, **140**, 1756–1770, doi:10.1002/qj.2261.

Mlawer, E. J., S. J. Taubman, P. D. Brown, M. J. Iacono, and S. A. Clough, 1997: Radiative transfer for inhomogeneous atmospheres: RRTM, a validated correlated-k model for the longwave. *J. Geophys. Res.*, **102**, 16 663–16 682, doi:10.1029/97JD00237.

Molinari, J., and D. Vollaro, 2010: Rapid intensification of a sheared tropical storm. *Mon. Wea. Rev.*, **138**, 3869–3885, doi:10.1175/2010MWR3378.1.

——, ——, and K. L. Corbosiero, 2004: Tropical cyclone formation in a sheared environment: A case study. *J. Atmos. Sci.*, **61**, 2493–2509, doi:10.1175/JAS3291.1.

——, P. Dodge, D. Vollaro, K. L. Corbosiero, and F. Marks, 2006: Mesoscale aspects of the downshear reformation of a tropical cyclone. *J. Atmos. Sci.*, **63**, 341–354, doi:10.1175/JAS3591.1.

——, D. M. Romps, D. Vollaro, and L. Nguyen, 2012: CAPE in tropical cyclones. *J. Atmos. Sci.*, **69**, 2452–2463, doi:10.1175/JAS-D-11-0254.1.

——, J. Frank, and D. Vollaro, 2013: Convective bursts, downdraft cooling, and boundary layer recovery in a sheared tropical storm. *Mon. Wea. Rev.*, **141**, 1048–1060, doi:10.1175/MWR-D-12-00135.1.

Möller, J. D., and M. T. Montgomery, 2000: Tropical cyclone evolution via potential vorticity anomalies in a three-dimensional balance model. *J. Atmos. Sci.*, **57**, 3366–3387, doi:10.1175/1520-0469(2000)057<3366:TCEVPV>2.0.CO;2.

Montgomery, M. T., and R. J. Kallenbach, 1997: A theory for vortex Rossby waves and its application to spiral bands and intensity changes in hurricanes. *Quart. J. Roy. Meteor. Soc.*, **123**, 435–465, doi:10.1002/qj.49712353810.

——, and R. K. Smith, 2012: Paradigms for tropical cyclone intensification. Ludwig Maximilians University of Munich Meteorological Institute Tropical Cyclone Research Rep. 1, 29 pp.

——, M. E. Nicholls, T. A. Cram, and A. B. Saunders, 2006: A vortical hot tower route to tropical cyclogenesis. *J. Atmos. Sci.*, **63**, 355–386, doi:10.1175/JAS3604.1.

Nguyen, L. T., J. Molinari, and D. Thomas, 2014: Evaluation of tropical cyclone center identification methods in numerical models. *Mon. Wea. Rev.*, **142**, 4326–4339, doi:10.1175/MWR-D-14-00044.1.

Noh, Y., W. G. Cheon, S. Y. Hong, and S. Raasch, 2003: Improvement of the K-profile model for the planetary boundary layer based on large eddy simulation data. *Bound.-Layer Meteor.*, **107**, 401–427, doi:10.1023/A:1022146015946.

Nolan, D. S., 2007: What is the trigger for tropical cyclogenesis? *Aust. Meteor. Mag.*, **56**, 241–266.

——, 2011: Evaluating environmental favorableness for tropical cyclone development with the method of point-downscaling. *J. Adv. Model. Earth Syst.*, **3**, M08001, doi:10.1029/2011MS000063.

——, Y. Moon, and D. P. Stern, 2007: Tropical cyclone intensification from asymmetric convection: Energetics and efficiency. *J. Atmos. Sci.*, **64**, 3377–3405, doi:10.1175/JAS3988.1.

Onderlinde, M. J., and D. S. Nolan, 2014: Environmental helicity and its effects on development and intensification of tropical cyclones. *J. Atmos. Sci.*, **71**, 4308–4320, doi:10.1175/JAS-D-14-0085.1.

Pendergrass, A. G., and H. E. Willoughby, 2009: Diabatically induced secondary flows in tropical cyclones. Part I: Quasi-steady forcing. *Mon. Wea. Rev.*, **137**, 805–821, doi:10.1175/2008MWR2657.1.

Rappin, E. D., D. S. Nolan, and K. A. Emanuel, 2010: Thermodynamic control of tropical cyclogenesis in environments of radiative-convective equilibrium with shear. *Quart. J. Roy. Meteor. Soc.*, **136**, 1954–1971, doi:10.1002/qj.706.

Raymond, D. J., and S. L. Sessions, 2007: Evolution of convection during tropical cyclogenesis. *Geophys. Res. Lett.*, **34**, L06811, doi:10.1029/2006GL028607.

——, ——, and Ž. Fuchs, 2007: A theory for the spinup of tropical depressions. *Quart. J. Roy. Meteor. Soc.*, **133**, 1743–1754, doi:10.1002/qj.125.

——, ——, and C. López Carrillo, 2011: Thermodynamics of tropical cyclogenesis in the northwest Pacific. *J. Geophys. Res.*, **116**, D18101, doi:10.1029/2011JD015624.

Reasor, P. D., and M. T. Montgomery, 2001: Three-dimensional alignment and corotation of weak, TC-like vortices via linear vortex Rossby waves. *J. Atmos. Sci.*, **58**, 2306–2330, doi:10.1175/1520-0469(2001)058<2306:TDAACO>2.0.CO;2.

——, and M. D. Eastin, 2012: Rapidly intensifying Hurricane Guillermo (1997). Part II: Resilience in shear. *Mon. Wea. Rev.*, **140**, 425–444, doi:10.1175/MWR-D-11-00080.1.

——, M. T. Montgomery, and L. D. Grasso, 2004: A new look at the problem of tropical cyclones in vertical shear flow: Vortex resiliency. *J. Atmos. Sci.*, **61**, 3–22, doi:10.1175/1520-0469(2004)061<0003:ANLATP>2.0.CO;2.

——, R. Rogers, and S. Lorsolo, 2013: Environmental flow impacts on tropical cyclone structure diagnosed from airborne Doppler radar composites. *Mon. Wea. Rev.*, **141**, 2949–2969, doi:10.1175/MWR-D-12-00334.1.

Riemer, M., M. T. Montgomery, and M. E. Nicholls, 2010: A new paradigm for intensity modification of tropical cyclones: Thermodynamics impact of vertical wind shear on the inflow layer. *Atmos. Chem. Phys.*, **10**, 3163–3188, doi:10.5194/acp-10-3163-2010.

Rogers, R., P. Reasor, and S. Lorsolo, 2013: Airborne Doppler observations of the inner-core structural differences between intensifying and steady-state tropical cyclones. *Mon. Wea. Rev.*, **141**, 2970–2991, doi:10.1175/MWR-D-12-00357.1.

——, ——, and J. A. Zhang, 2015: Multiscale structure and evolution of Hurricane Earl (2010) during rapid intensification. *Mon. Wea. Rev.*, **143**, 536–562, doi:10.1175/MWR-D-14-00175.1.

Romps, D. M., and Z. Kuang, 2010: Do undiluted convective plumes exist in the upper tropical troposphere? *J. Atmos. Sci.*, **67**, 468–484, doi:10.1175/2009JAS3184.1.

Rozoff, C. M., W. H. Schubert, B. D. McNoldy, and J. P. Kossin, 2006: Rapid filamentation zones in intense tropical cyclones. *J. Atmos. Sci.*, **63**, 325–340, doi:10.1175/JAS3595.1.

Simpson, R., and R. Riehl, 1958: Mid-tropospheric ventilation as a constraint on hurricane development and maintenance. Preprints, *Tech. Conf. on Hurricanes*, Miami Beach, FL, Amer. Meteor. Soc., D4-1–D4-10.

Skamarock, W. C., and Coauthors, 2008: A description of the Advanced Research WRF version 3. NCAR Tech. Note NCAR/TN-475+STR, 113 pp. [Available online at http://www.mmm.ucar.edu/wrf/users/docs/arw_v3_bw.pdf.]

Smith, R. K., M. T. Montgomery, and S. V. Nguyen, 2009: Tropical cyclone spinup revisited. *Quart. J. Roy. Meteor. Soc.*, **135**, 1321–1335, doi:10.1002/qj.428.

Tang, B., and K. Emanuel, 2010: Midlevel ventilation's constraint on tropical cyclone intensity. *J. Atmos. Sci.*, **67**, 1817–1830, doi:10.1175/2010JAS3318.1.

Van Sang, N., R. K. Smith, and M. T. Montgomery, 2008: Tropical-cyclone intensification and predictability in three dimensions. *Quart. J. Roy. Meteor. Soc.*, **134**, 563–582, doi:10.1002/qj.235.

Vigh, J. L., and W. H. Schubert, 2009: Rapid development of the tropical cyclone warm core. *J. Atmos. Sci.*, **66**, 3335–3350, doi:10.1175/2009JAS3092.1.

Wang, Z., M. T. Montgomery, and T. J. Dunkerton, 2010: Genesis of pre–Hurricane Felix (2007). Part I: The role of the easterly wave critical layer. *J. Atmos. Sci.*, **67**, 1711–1729, doi:10.1175/2009JAS3420.1.

Zhang, D.-L., Y. Liu, and M. K. Yau, 2002: A multiscale numerical study of Hurricane Andrew (1992). Part V: Inner-core thermodynamics. *Mon. Wea. Rev.*, **130**, 2745–2763, doi:10.1175/1520-0493(2002)130<2745:AMNSOH>2.0.CO;2.

Zhang, F., and D. Tao, 2013: Effects of vertical wind shear on the predictability of tropical cyclones. *J. Atmos. Sci.*, **70**, 975–983, doi:10.1175/JAS-D-12-0133.1.

Zhang, J. A., R. F. Rogers, P. D. Reasor, E. W. Uhlhorn, and F. D. Marks Jr., 2013: Asymmetric hurricane boundary layer structure from dropsonde composites in relation to the environmental vertical wind shear. *Mon. Wea. Rev.*, **141**, 3968–3984, doi:10.1175/MWR-D-12-00335.1.